Estuarine, Coastal and Shelf Science 266 (2022) 107664

Contents lists available at ScienceDirect

Estuarine, Coastal and Shelf Science

journal homepage: www.elsevier.com/locate/ecss

Exploring open-source multispectral satellite remote sensing as a tool to map long-term evolution of salt marsh shorelines

Tegan R. Blount [a,b,c,*], A. Rita Carrasco [b], Sónia Cristina [b], Sonia Silvestri [c]

[a] Murray Foundation, Brabners LLP, Horton House, Exchange Street, Liverpool, L2 3YL, United Kingdom
[b] CIMA - Centre for Marine and Environmental Research, Universidade do Algarve, Campus de Gambelas, 8005-139 Faro, Portugal
[c] Department of Biological, Geological, and Environmental Sciences, University of Bologna, Campus of Ravenna, Italy

ARTICLE INFO

Keywords:
Multispectral satellite
Salt marsh
Transitional zones
Shoreline evolution
Wetland mapping
Ria Formosa Lagoon

ABSTRACT

From an ecological and socio-economic perspective, salt marshes are one of the most valuable natural assets on Earth. As external pressures are causing their extensive degradation and loss globally, the ability to monitor salt marshes on a long-term scale and identify drivers of change is essential for their conservation. Remote sensing has been demonstrated to be one of the most adept methods for this purpose and open-source multispectral satellite remote sensing missions have the potential to provide worldwide long-term time-series coverage that is non-cost-prohibitive. This study derives the long-term lateral evolution of four salt marsh patches in the Ria Formosa coastal lagoon (Portugal) using data from the Sentinel-2 and Landsat missions as well as from aerial photography surveys to quantitatively examine the accuracy and associated uncertainty in using open-source multispectral satellite remote sensing for this purpose. The results show that these open-source satellite archives can be a useful tool for tracking long-term salt marsh extent dynamics. During 1976–2020, there was a net loss of salt marsh in the study area, with erosion rates reaching an average of −3.3 m/yr opposite a tidal inlet. The main source of error in the satellite results was the dataset spatial resolution limits, but the specific salt marsh shoreline environment contributed to the relative magnitude of that error. The study notes the influence of eco-geomorphological dynamics on the mapping of sedimentary environments, so far not extensively discussed in scientific literature, highlighting the difference between mapping a morphological process and a sedimentary environment.

1. Introduction

Salt marshes are a component of the coastal intertidal zone. Geographically, they are present from the Arctic to the subtropical latitudes in sheltered intertidal areas, but they are most abundant in temperate zones (Mcowen et al., 2017). They are characterised by periodically inundated vegetated platforms incised with a dendritic network of tidal channels and have highly complex eco-geomorphodynamics shaped by interrelationships between biological and physical mechanisms (D'Alpaos, 2011; D'Alpaos and Marani, 2016; Marani et al., 2006a).

Salt marshes have a considerable ecological influence on both terrestrial and marine systems and thus, the socio-economic system. They are multifunctional sites of intense primary and secondary production (Barbier et al., 2011; Vernberg, 1993), key biodiversity habitats (Gopi et al., 2019; Mitsch and Gosselink, 2015), contributors to coastal flood defence services (Hoggart et al., 2015; Reed et al., 2018), fixers of heavy metals (Moreira Da Silva et al., 2015; Reboreda and Caçador, 2007) and sinks for atmospheric carbon and nutrients (Caçador et al., 2016; Lillebø et al., 2010; Sousa et al., 2010). Amongst other ecosystem services, salt marshes are also sites of cultural, recreational and scientific importance (Barbier et al., 2011; Costanza et al., 1997; Newton et al., 2018).

Salt marshes are dynamic, valuable and vulnerable ecosystems for which monitoring is a fundamental necessity, yet highly challenging *in situ* due to their large surface area to vertical relief ratio and poor accessibility (Silvestri et al., 2003). Despite the great ecological significance of the salt marsh ecosystem, they are not always sufficiently protected (Himes-Cornell et al., 2018; Materu et al., 2018; Rogers et al., 2016). Due to pressures from the environmental drivers and anthropogenic activities concentrated in the coastal zone, such as sea-level rise and channel dredging, salt marsh ecosystems have sustained great losses

* Corresponding author. CIMA - Centre for Marine and Environmental Research, Universidade do Algarve, Campus de Gambelas, 8005-139 Faro, Portugal.
E-mail address: a66253@ualg.pt (T.R. Blount).

https://doi.org/10.1016/j.ecss.2021.107664
Received 29 March 2021; Received in revised form 17 September 2021; Accepted 17 November 2021
Available online 27 November 2021

and remain under significant threat (Gu et al., 2018; Silvestri et al., 2018; Valiela et al., 2009, 2018).

Remote sensing allows the collection of global datasets that aid spatial and temporal understanding of the Earth as a system and the complex interrelations within it from afar and in a cost-effective way (Qu et al., 2006). Remote sensing can enable effective and informed environmental policy and legislation (El Mahrad et al., 2020; Maes et al., 2020). It has been demonstrated to support the implementation of the European Water Framework Directive (Best et al., 2007; Brito et al., 2012) and the Ramsar Convention on Wetlands (Chasmer et al., 2020a, 2020b). It is also vital to ecosystem-based management approaches (Nayak, 2004; Ouellette and Getinet, 2016).

As a technique, remote sensing has its constraints; it requires reliable control points for georectification and is reliant on other forms of data for validation, and supplementation where necessary (e.g. Darvishzadeh et al., 2019; Taramelli et al., 2018). It also needs frameworks and platforms for data processing and storage, and even though remote sensing is a cost-effective method compared to *in situ* data collection, using remote sensing data like aerial photography may still be cost-prohibitive (Mumby et al., 1999; Read et al., 2020). Furthermore, the focus of a study must be of a matching temporal, spatial and spectral resolution as the remote sensing data, which can be challenging to satisfy in the dynamic coastal zone. Finally, cloud coverage, inundation and waves can be sources of error and render large amounts of remote sensing data unusable (e.g. Campbell and Wang, 2018; Canisius et al., 2019; Silvestri et al., 2003). Thus, it is vital to select a remote sensing technique that is suitable for the study target system and objectives.

In this study, we evaluate the potential of using the multispectral satellite remote sensing data from open-source missions for salt marsh shoreline mapping and long-term evolution tracking. The objectives of this study are to (1) derive long-term salt marsh shoreline evolutionary trends in a sector of the Ria Formosa coastal lagoon; (2) undertake a sensitive analysis of the relative accuracy of the satellite remote sensing results compared to a commonly implemented higher spatial resolution remote sensing technology, aerial photography; and (3) investigate the relative shoreline mapping performance of current contemporaneous sensors Landsat-8 and Sentinel-2 to explore the suitability of integrating their datasets in a salt marsh shoreline monitoring context.

2. Satellite remote sensing data and application in salt marsh mapping

Satellite remote sensing, a remote sensing technique where data is acquired by a sensor on a satellite platform orbiting the Earth, has the potential to become one of the most useful tools to delineate and monitor the long-term evolution of salt marshes. The key advantage of satellite remote sensing is that it provides instantaneous data covering large areas, is repeatable and data gathering can be rapid, frequent and multidecadal. These attributes give satellite remote sensing an advantage over aerial photographs, as although they are of higher resolution, aerial photography repositories are globally sparse in their coverage, sporadic in revisit frequency, variable in resolution and cost to access.

Over time, advancement in satellite remote sensing technologies has been accompanied by advancements in software and algorithm development as well as the advent of cloud computing and open-source archives where satellite remote sensing data is freely available (e.g. DeLancey et al., 2019; Mahdianpari et al., 2019; Zhu et al., 2019). This, coupled with an increasing awareness of the value and vulnerability of coastal ecosystems, has meant that research applying satellite remote sensing to salt marshes has grown in recent times. As a result, progressively more elegant solutions for mapping and monitoring the dynamics of increasingly diverse and indirect properties of salt marshes have been developed (e.g. Da Lio et al., 2018; Eon et al., 2019; Taramelli et al., 2018). Currently, salt marsh shoreline delineation studies rely on expert visual interpretation or classification techniques, or a combination of both (e.g. Farris et al., 2019; Lopes et al., 2020; Sun et al., 2017). In semi-automated or automated shoreline delineation methodologies, some form of decision tree classification by spectral feature analysis is employed depending on the particular study's requirements and constraints (e.g. Klemas, 2011; Laengner et al., 2019; Niu et al., 2012).

To improve delineation accuracy, satellite remote sensing data can be integrated with a wide range of additional data sources including different classes of remote sensors (e.g. Darvishzadeh et al., 2019; Marani et al., 2006b; Tian et al., 2015). Although significant progress has been made towards accurate standardised satellite remote sensing based automated continent to global level salt marsh mapping and monitoring (e.g. Laengner et al., 2019; Mcowen et al., 2017; Reschke and Hüttich, 2014), it is not fully resolved (Guo et al., 2017; Wu, 2018). A lack of calibration between sensors and spatial resolution limits can restrict the extent of time-series and thus the ability to derive long-term trends (e.g. Campbell and Wang, 2020; Lopes et al., 2019; Wu, 2019). Furthermore, although most studies undertake an accuracy assessment, there is a general lack of cross comparability between the studies' measures of accuracy, which can be a barrier to the widespread uptake of satellite remote sensing in operational coastal management (Chasmer et al., 2020a).

Spanning almost fifty years, the Landsat programme has risen to prominence as one of the most valuable sources for Earth Observations, especially for time-series analysis (Holden and Woodcock, 2016; Li et al., 2019). The Landsat programme began with Landsat-1 in 1972 and the most recent mission, Landsat-8, was launched in 2013. As a result of technological advancements during this period, the revisit frequency and the spectral and spatial resolution of the Landsat multispectral imagery improves through time. Operating since 2015, the Copernicus programme's Sentinel-2 mission has twin satellites, 2A and 2B, and the highest spatial resolution and revisit frequency of the current multispectral open-source satellites. Combining the Landsat archive with that of the Sentinel-2 mission results in unrivalled coverage of the Earth, which is non-cost-prohibitive, frequent, ongoing, standardised, medium to high spatial resolution and multi-decadal in duration. The temporal duration of this archive is sufficient to allow the derivation of nuanced long-term system dynamics and to locate socio-economic and biophysical drivers of coastal ecosystem change (Barbosa et al., 2015; Knight et al., 1997; Vernberg, 1993). Long-term time-series are vital for assessing salt marsh degradation as these resilient systems may only exhibit minor yearly shoreline changes. Focusing on mapping the salt marsh extents enables the assessment of key indicators of salt marsh degradation such as edge erosion and area loss from drowning. Although the spatial resolution of open-source multispectral satellite sensors can limit the fine-scale accuracy of tools based on their data, their accuracy and spatiotemporal coverage is useful for many ecosystem management applications (Reschke and Hüttich, 2014; Waldner et al., 2018). Since salt marshes are generally data-poor and insufficiently studied on a long-term scale (Wu, 2018), both the research and coastal management fields can benefit significantly from the potential of open-source multispectral satellite remote sensing data to aid spatiotemporal understanding of this complex and dynamic ecosystem (Maes et al., 2020; Qu et al., 2006).

As far as we are aware, it is unprecedented to combine all the Landsat multispectral sensors in a long-term time-series to examine salt marsh shoreline morphological trends. Nor are we aware of any studies that compare the relative accuracy of these satellite remote sensing derived salt marsh shorelines and evolutionary trends with those derived from aerial photography. Studies focusing on validation and cross-compatibility of satellite remote sensing data are vital for progressing salt marsh scientific research and management (Congalton and Green, 2019). By quantifying the satellite remote sensing relative accuracy, the limitations of using the complete Landsat and Sentinel-2 archive for deriving salt marsh shorelines and long-term morphological evolution can be defined, along with exploring the interplay between spatial resolution and shoreline environment. Also, by comparing the salt marsh shoreline mapping capability of Landsat-8 with Sentinel-2, the effects of

integrating these contemporary missions in salt marsh shoreline studies to enhance the spatial resolution and revisit frequency of the open-source archive will be clarified. Furthermore, this study supports the current need to map and monitor a wide range of salt marshes from different climatic regions to improve the accuracy of global level automated salt marsh mapping mechanisms (Lopes et al., 2019) and addresses issues limiting the application of satellite datasets in coastal management (El Mahrad et al., 2020). The satellite remote sensing method employed herein is designed to be open-access, neither cost nor processing power prohibitive, geographically translatable and not reliant on high levels of technical expertise to implement.

3. Methods

3.1. Study area

The Ria Formosa lagoon, located on the southern coast of Portugal (Fig. 1), is a multi-barrier coastal lagoon system with five barrier islands and two sandspit peninsulas which are dynamic but resilient (Kombiadou et al., 2018). The enclosed lagoon system is almost 55 km long, up to 6 km wide and rests on a geological basement of barrier platform sand (Bettencourt, 1994). The system compromises six tidal inlets and the western sector tidal prism revolves around the Faro-Olhão, Armona and Ancão inlets (Cravo et al., 2014). The maximum tidal range is 3.5 m and the average tidal ranges are from 1.3 m in neap to 2.8 m in spring (Pacheco et al., 2008). Any fluvial sources of fresh-water or sediment are minor (Andrade, 1990). The average depth of the lagoon is 2 m and intertidal geomorphological features are salt marshes, tidal flats and complex channel networks which cumulatively cover 90% of the lagoon's surface (Andrade et al., 2004).

Salt marsh development in the Ria Formosa lagoon began from the middle Holocene (Sousa et al., 2019). Within the Ria Formosa, the salt marsh vegetation species distribution is affected by the submergence duration and estuarine gradient (Arnaud-Fassetta et al., 2006), as well as the frequency of inundation (Balke et al., 2016) and specific soil conditions (Contreras-Cruzado et al., 2017). There is a wide variety of intertidal vegetation species present in the lagoon (Costa et al., 1996). The most frequently encountered species on the salt marsh shoreline are *Spartina maritima*, *Sarcocornia perennis* and *Puccinellietum convolutae* (Arnaud-Fassetta et al., 2006; Bertrand et al., 2003; Contreras-Cruzado et al., 2017; Costa et al., 1996). On the adjacent tidal flats, *Zostera noltii* is commonly found at times interspersed with colonising clumps of *Spartina maritima* and *Sarcocornia perennis*. Examples of characteristic salt marsh morphology and vegetation in the Ria Formosa are presented in Appendix A (Fig. A.1).

The salt marshes examined in this study are located in the centre of the lagoon and comprise the North, South, East and West salt marsh patches (Fig. 1). These salt marshes are bounded by tidal flats (vegetated with seagrasses or non-vegetated), lagoon (estuarine) channels and marsh detached beaches (Carrasco et al., 2021). The central salt marshes were chosen since they are representative of stable salt marshes less influenced by the tidal inlets and are therefore more suitable for an overall comparison tracking salt marsh long-term natural dynamics.

The Ria Formosa is a vital habitat for globally threatened species (Correia et al., 2015; Siegenthaler et al., 2015) and provides many ecosystem services, especially the regulating and cultural services (Newton et al., 2018). As a lagoon system, the Ria Formosa has natural stressors (Mateus et al., 2016) and these are compounded by additional anthropogenic pressures. The lagoon system is complex and sensitive (Cravo et al., 2014), influenced by past land reclamations (Sousa et al., 2020), inlet stabilisations (Kombiadou et al., 2018) and the dredging of navigable channels (Arnaud-Fassetta et al., 2006). These human interventions have modified the system's hydrodynamic and sediment regime and identified consequences for the lagoon salt marshes include localised shoreline erosion and increased vulnerability to sea-level-rise (Carrasco et al., 2021).

3.2. Salt marsh shoreline identification and mapping

Four pairs of aerial and Landsat images were used, collected between 1976 and 2014, alongside three pairs of Landsat-8 and Sentinel-2 images collected between 2016 and 2020. The aerial photography images for

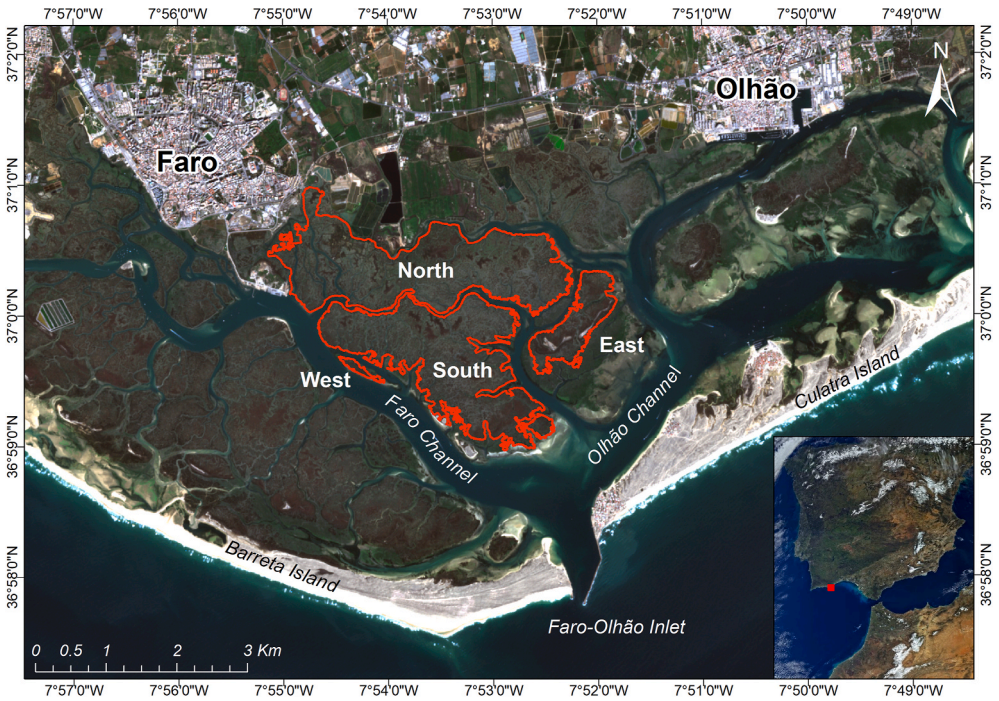

Fig. 1. The geographic location of the salt marsh study site in central Ria Formosa coastal lagoon (Portugal) (the main image contains modified [Blount, 2020] Sentinel-2B Level 2A data [24-02-2020], processed by the European Space Agency (ESA); the overview image contains water colour enhanced ML Sentinel-3 OLCI [1-03-2016], processed by ESA). (For interpretation of the references to colour in this figure legend, the reader is referred to the Web version of this article.)

2002 and 2014 were orthophotograph mosaics while the images from 1976 to 1989 were individually scanned into digital format. The Landsat satellite images were extracted from the United States Geological Survey (USGS) Earth Explorer archive (https://earthexplorer.usgs.gov/). From 1989 onwards, the Landsat images were Collection 1 Landsat Level 2 Tier 1 products, corrected to surface reflectance as per USGS standard and suitable for time-series analyses (U.S. Geological Survey, 2019a; 2019b, 2019c). Due to lack of an alternative, the Landsat-1 1976 image was a legacy terrain corrected product (U.S. Geological Survey, 2018). Any lower-quality image registration this entailed was accommodated for in the study's methodology (U.S. Geological Survey, 2019c). The Sentinel-2 images for 2016, 2018 and 2020 were sourced from the Copernicus Open Access Hub (https://cophub.copernicus.eu/dhus/#/home). The Sentinel-2 data was atmospherically corrected to land surface reflectance (Level 2A) (Louis, 2017). Three GPS transects intersecting the salt marsh shoreline in the study area were used for ground truthing. The remote sensing and field datasets used in this study are fully described in Appendix B (section B.1, Table B.1 and section B.2).

Visual assessment of a variety of raster display band combinations and indexes was undertaken to ascertain which was the most adapted for visual salt marsh shoreline delineation in the context of a multi-sensor long-term time-series. Out of all the trialled band combinations, the colour-infrared demonstrated superior visual distinction of the intertidal morphologies and vegetation classes. Of the indexes, the Normalised Difference Vegetation Index (NDVI) performed the best but was still outperformed by colour-infrared and natural colour as it did not distinguish between certain coastal morphologies important to this study. The above, combined with the fact that some of the Landsat missions in the time-series do not have a blue band, made the colour-infrared band combination the best option for the visual delineation of salt marshes in the context of this study. The choice of colour-infrared, leveraging the near-infrared, red and green bands, was as per recommendations from other salt marsh vegetation studies (Kelly et al., 2011; Silvestri et al., 2003). Since the salt marsh shorelines at the study site are usually either adjacent to tidal flats (vegetated or non-vegetated) or marsh detached beaches, discerning the boundary between these morphologies was the priority for shoreline identification. The morphological criteria used for salt marsh shoreline delineation on aerial and satellite imagery are described in Supplementary Material, Table S.1. Additional morphological criteria (Supplementary Material, Table S.2) were used for satellite imagery salt marsh shoreline delineation in transitional zones and narrow estuarine channels, as these morphologies had a notable effect on the satellite imagery shoreline accuracy.

The salt marsh shorelines were delineated by hand as line features in the GIS environment using expert visual interpretation for each remote sensing image (Appendix B, section B.1, Table B.1). The mapped shoreline positions were validated using data from literature and fieldwork undertaken prior to this study (Appendix C, section C.1, Table C.1 and Fig. C.1). Three topographic transects were overlaid with the satellite imagery and aerial photography shoreline intersection points. Horizontal zonation and elevation ranges were deduced for the target salt marsh bionomic levels, also based on earlier marsh platform analysis (Arnaud-Fassetta et al., 2006). In the absence of specific field data defining the lateral shoreline position, the bionomic ranges served to identify the approximate boundaries of the lower, middle and high salt marsh zones and hence the position of the salt marsh shoreline on the transects. The term "low marsh" in this context pertains to the transitional zone where isolated salt marsh colonies are present on the tidal flats, at times intermixed with seagrass meadows.

3.3. Salt marsh shoreline analysis

The shoreline trends and relative accuracy were assessed based on the analysis of salt marsh areas, perimeters, shoreline positions and rates-of-change. The salt marsh areas were included as an alternative method to track salt marsh evolution as opposed to shoreline rate-of-change focused time-series. The salt marsh perimeter and the perimeter-to-area ratio were included in the analysis because they can serve as proxy measures for salt marsh shoreline intricacy. Shoreline intricacy can be an indicator of ecosystem fragmentation (Rebelo et al., 2017), erosion rate magnitude (Leonardi et al., 2016) and a measure of the delineation capability for each satellite sensor.

The Digital Shoreline Analysis System (DSAS; v.5.0 software; Himmelstoss et al., 2018b, 2018a) was employed to undertake the shoreline rate and comparison analysis. Transects were cast every 25 m along the shorelines as it was found to be an optimal spacing from a computational and geometric perspective (i.e., the observed level of shoreline complexity). The confidence interval of the regression rates was 90%. The shoreline location uncertainty (Morton et al., 2004) was calculated for each of the ten digitalised salt marsh shorelines. The method used for calculating shoreline uncertainty was aligned with that of other DSAS shoreline studies in the Ria Formosa (e.g. Carrasco et al., 2021; Kombiadou et al., 2018). The digitalisation error for the satellite imagery was taken as the pixel size instead of four times the pixel size, as is standard for aerial photography (Jabaloy-Sánchez et al., 2014), since the satellite imagery shoreline delineation was undertaken at full-resolution zoom.

The DSAS analysis calculated the following statistics: Net Shoreline Movement (NSM), End Point Rate (EPR) and Weighted Linear Regression (WLR) rate. The NSM reports the distance between the oldest and the youngest shorelines while the EPR is derived by dividing the distance of shoreline movement by the time elapsed between the oldest and the youngest shoreline positions. The WLR rate determines a rate-of-change statistic by applying shoreline location uncertainty weightings and fitting a least squares regression to all shorelines at each transect. The EPR uncertainty is the square root of the summed squares of the two shoreline uncertainty values divided by the number of years between the shorelines (Himmelstoss et al., 2018b). The WLR uncertainty is the regionally averaged 90% confidence interval on the linear regression line (Ruggiero et al., 2013). Himmelstoss et al. (2018b) provides a detailed guide to these statistics.

In this study, different rate methods were used as complementary tools. The NSM was used to directly compare the aerial photography and satellite imagery shorelines as well as compare the Sentinel-2 and Landsat-8 shorelines. The EPR was used to derive the medium-term shoreline trends for 1976–1989, 1989–2002 and 2002–2014, since these time-series held insufficient shorelines for the linear regression statistics to function. The long-term shoreline trend comparisons for 1976–2014, 1976–2020 and 1989–2014 were calculated using the established WLR rate, which takes account of all the shorelines and their positional uncertainties (Himmelstoss et al., 2018b; Morton et al., 2004). The period 1989–2014 is sub-quadridecadal but was included in the comparison analysis to investigate the effect that removing the lowest resolution image would have on the accuracy of the satellite remote sensing rate predictions.

4. Results

4.1. Salt marsh area and perimeter

The georeferencing results and the salt marsh shoreline accuracy, uncertainty and validation can be found in Appendix C (section C.1 and Fig. C.1). The salt marsh areas and perimeters derived from the delineated shorelines are shown in Fig. 2. The aerial photography marsh areas are almost constant over time, apart from the South marsh, that shows a decreasing trend during 1976–2014 indicative of notable salt marsh loss. Across all the salt marsh patches, the satellite imagery areas overestimate the aerial photography areas, but the magnitude of overestimation reduces from 1976 to 2014 (Fig. 2a). This indicates a substantial improvement in salt marsh edge detection accuracy by the satellite remote sensing method over time. The South marsh has the largest area overestimate and this falls from 0.26 km^2 to 0.02 km^2 during this period (Fig. 2a). The Landsat-8 areas were on average an

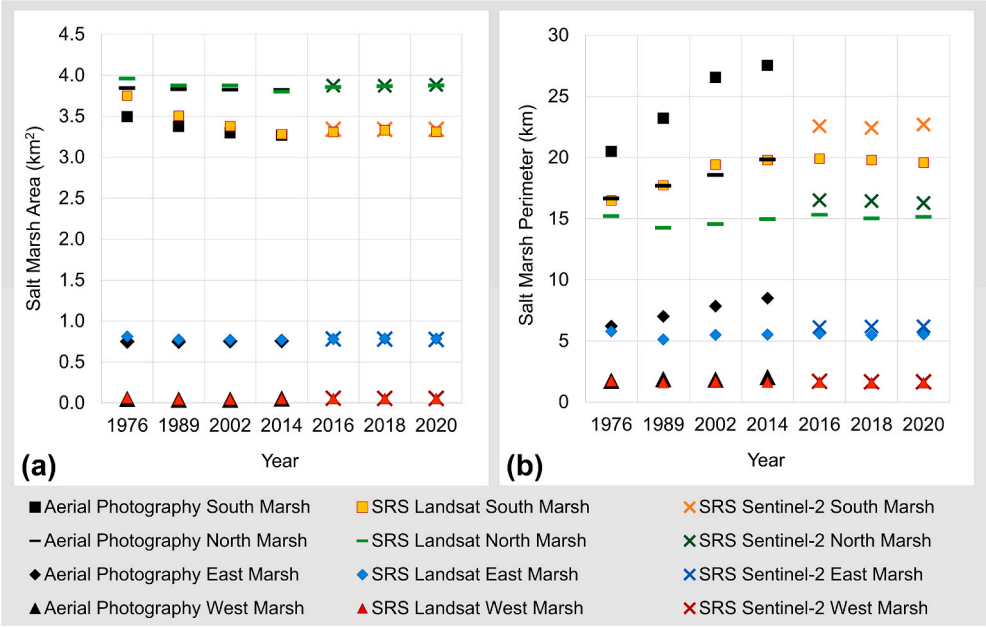

Fig. 2. Based on the shorelines delineated from satellite remote sensing (SRS) and aerial photography (AP) imagery for 1976, 1989, 2002, 2014, 2016, 2018 and 2020: (a) the areas of the North, East, West and South salt marshes; (b) the perimeters of the North, East, West and South salt marshes. The uncertainty of these areas and perimeters is related to the shoreline positional uncertainty as described in Section 3.2 and Appendix C.1.

underestimate of the Sentinel-2 areas, and this underestimate tended to increase slightly as the salt marsh area increased (Fig. 2a).

With regards to the perimeters, the higher the resolution of the image, the more accurate the delineation of shoreline intricacies. Thus, the aerial photography perimeters are longer than the satellite imagery perimeters and the Sentinel-2 perimeters are longer than the Landsat-8 perimeters. Despite this, the satellite perimeters increasingly underestimate the aerial photography perimeters during 1976–2014 (Fig. 2b). This is because the improvement in the satellite imagery shoreline accuracy is masked by the aerial photography rapidly gaining the spatial resolution where the transitional zone shoreline intricacies can be delineated in detail. The magnitude of the difference between the satellite imagery and aerial photography perimeters increases as the perimeter of the salt marsh increases, not as the total area of the salt marsh increases, hence the perimeter error is a function of length (Fig. 2b). The South marsh, which has the greatest portion of intricate transitional shoreline, has the greatest error with its relative perimeter underestimate increasing from 4.0 km to 7.7 km over this period (Fig. 2b).

The four salt marshes ranked by increasing perimeter-area ratio are North, South, East and West. The percentage by which the satellite imagery areas overestimate the aerial photography areas increases as the perimeter-area ratio increases for all years and the error rises more rapidly the lower the resolution of the dataset (Fig. 3). This finding confirms that the salt marsh perimeter-area ratio does have a direct effect on the area inaccuracies of the satellite remote sensing method.

4.2. *Salt marsh shoreline lateral position*

To gauge the shoreline delineation accuracy of the satellite remote sensing data, the position of the Landsat shorelines relative to contemporaneous aerial photography or Sentinel-2 shorelines was calculated. The aerial photography shorelines were the baseline for 1976, 1989, 2002 and 2014. Due to the unavailability of aerial imagery, the Sentinel-

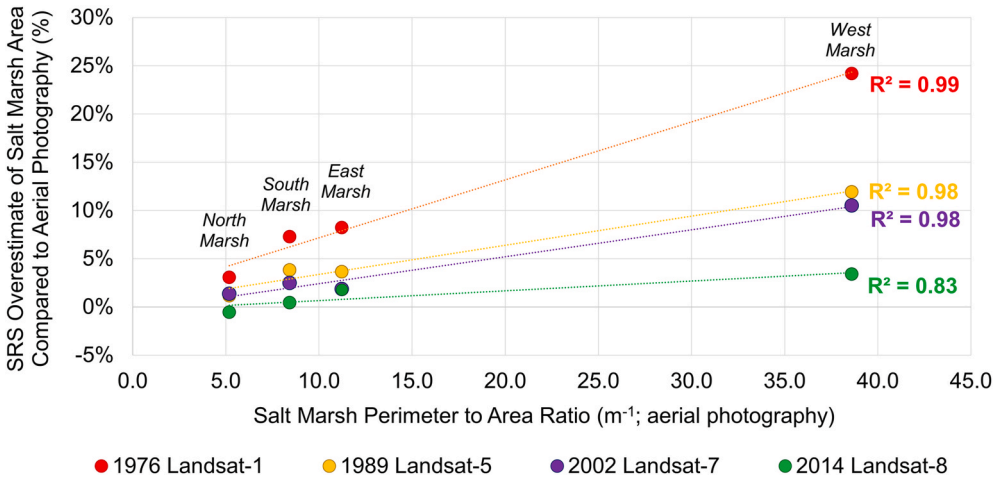

Fig. 3. The satellite remote sensing (SRS) salt marsh area percentage overestimate of the aerial photography (AP) areas plotted against the AP perimeter-area ratios of the North, East, West and South salt marsh in 1976, 1989, 2002 and 2014. The trendline coefficient of determination (R^2) has been included for each variable.

2 shorelines were the baseline for 2016, 2018 and 2020. The results are summarised in Fig. 4 and complementary data can be found in Appendix D, Fig. D.1.

The average and maximum distances by which the Landsat shorelines deviate from the baseline shoreline for each salt marsh are depicted in Fig. 4a. For the Sentinel-2 baseline case (2016–2020), the data was averaged across the three years. The results confirm that as the spatial resolution increases through time, the magnitude by which the Landsat shorelines err from the baselines decreases. The average Landsat shoreline offsets have a similar range of magnitudes on both sides of the baseline while the Landsat maximum shoreline offsets showed an increasing bias to inshore extremes post-1976. As the complexity and size of the salt marsh increases, so does the magnitude of the satellite imagery shoreline displacement error. The maximum shoreline errors corresponded to the marshes with the greatest extents of transitional zones and to a lesser extent, marsh detached beaches and estuarine channels (see Supplementary Material, Tables S.1 and S.2 for their morphological description). The standard deviation of the satellite imagery shoreline error also decreases over time (Fig. 4b). For each year the maximum standard deviation is approximately the satellite image pixel size, and the minimum standard deviation is close to half the satellite image pixel size. Notably, the 2014 Landsat-8 shoreline was on average 2.6 m inshore of the 2014 aerial photography shoreline and the 2016–2020 Landsat-8 shorelines were on average 1.8 m inshore of their comparative Sentinel-2 shorelines (Fig. 4). This suggests that on average the Sentinel-2 shorelines are positioned inshore of the actual shoreline, but to a lesser extent than is the case for Landsat-8 shorelines. Hence, the higher resolution of the Sentinel-2 sensor (10 m) appears to allow better detection of the more offshore fragmented salt marsh shorelines.

Although there is variability in the accuracy of the long-term rates derived from the satellite imagery shorelines, in general the aerial photography 1976–2014 WLR rates (Fig. 5a) are well approximated by the satellite imagery 1976–2014 WLR rates (Fig. 5b). Comparatively, the satellite imagery 1989–2014 WLR rates (Fig. 5d) have a slightly improved level of accuracy relative to the aerial photography 1989–2014 WLR rates (Fig. 5c). The erosion bias visible in these satellite long-term time-series was less pronounced in the satellite imagery 1976–2020 WLR rates (Fig. 5e). Ranging between −2.5 and −5.7 m/yr, the satellite imagery rate of erosion at the toe of the South marsh for both 1976–2014 and 1989–2014 mimics the aerial photography values well. In addition, a close match between the satellite imagery and aerial photography WLR rates was not restricted to areas with high rates-of-change. The accreting section of the West marsh, which is adjacent to the South marsh, ranges from 0.5 to 3.0 m/yr and the satellite imagery rates for both 1976–2014 and 1989–2014 align well with the aerial photography rates. There are, however, cases where the satellite imagery WLR does not perform so well for minor rates-of-change and there are outlier rates-of-change present in the transition zones that are unmatched in the aerial photography rates. The top left of the North marsh is an example of this latter phenomenon causing large faux erosion and accretion rates (Fig. 5b).

In 1976–1989, the satellite EPR shoreline rates are heavily exaggerated and barely approximate the aerial photography EPR (Appendix D, Table D.1 and Fig. D.2). By the next time step, 1989–2002, the satellite imagery EPR shows significant improvement compared to aerial photography EPR as the rate uncertainty reduces by roughly half. The satellite imagery 2002–2014 EPR results show further improved accuracy and uniformity in approximating the aerial photography EPR

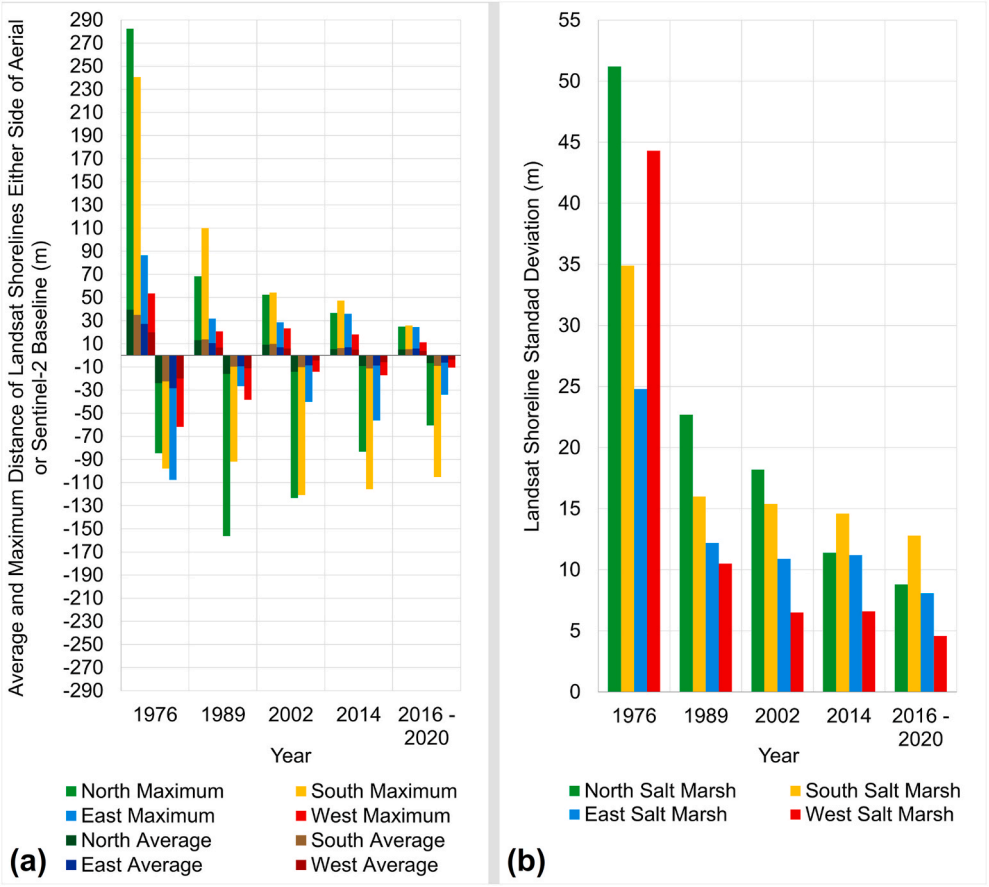

Fig. 4. For the North, South, East and West marshes: (a) the average and maximum distance of the Landsat satellite remote sensing (SRS) shoreline on either side of the baseline (positive distance indicates that the Landsat shorelines are offshore of the baseline); (b) the standard deviation of the distance between the Landsat and baseline shorelines. Aerial photography shorelines are the baselines for 1976–2014 and Sentinel-2 shorelines are the baselines for 2016–2020.

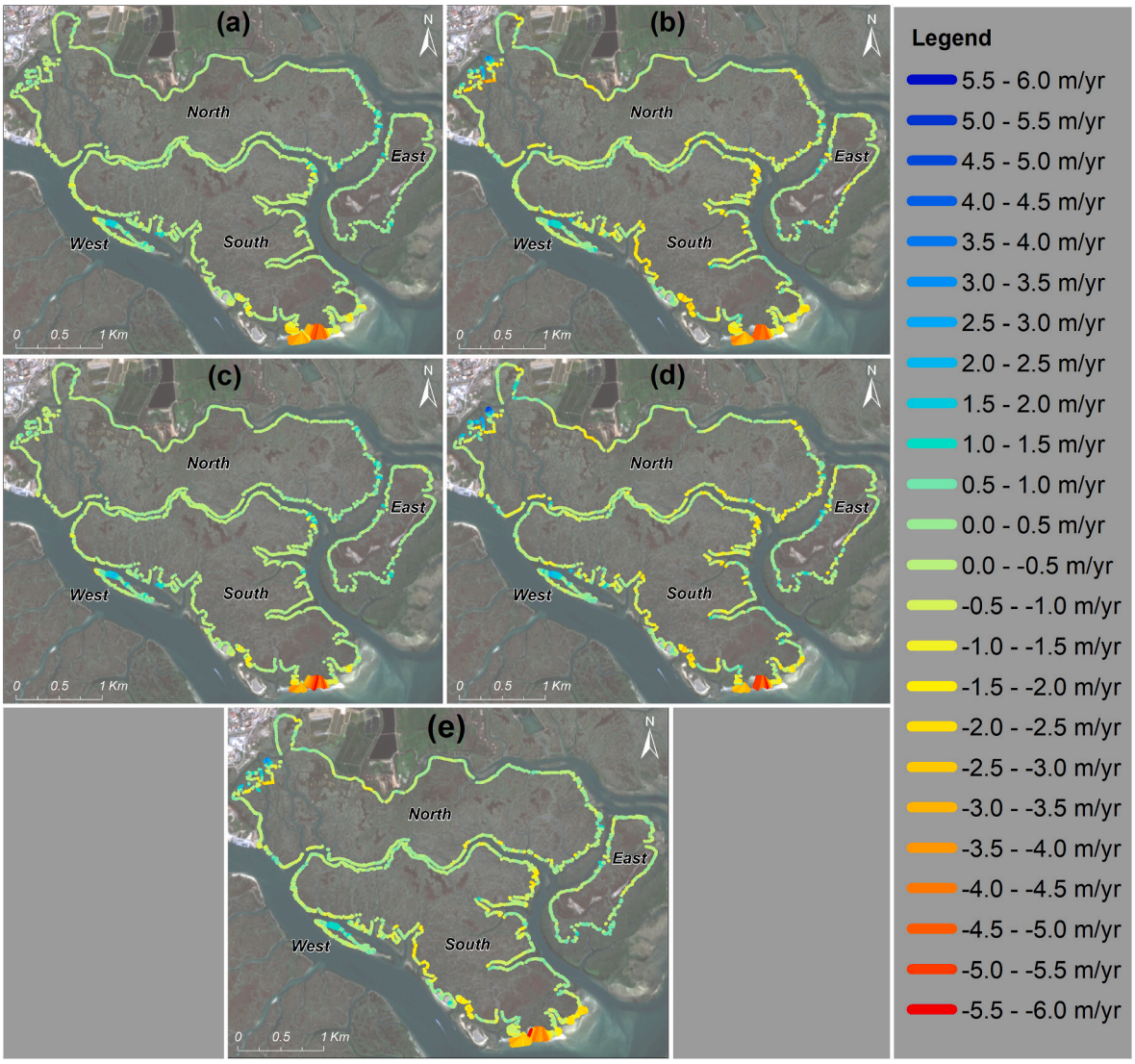

Fig. 5. Maps depicting salt marsh shoreline weighted linear regression (WLR) rates (m/yr) for the following time-series: (a) aerial photography (AP) 1976–2014; (b) satellite remote sensing (SRS) 1976–2014; (c) AP 1989–2014; (d) SRS 1989–2014; (e) SRS 1976–2020. ([Blount, 2020], contains modified Copernicus Sentinel-2B data [24-02-2020], processed by ESA).

rates. The erosive area at the toe of the South marsh is detected by the EPR for all periods but the 1976–1989 EPR is excessive by several magnitudes, as observable in the maximum satellite imagery rate of erosion in Table D.1 (Appendix D). The later satellite imagery EPRs 1989–2002 and 2002–2014 match the equivalent aerial photography EPR South toe erosion relatively well. The South toe is eroding non-linearly through time with the highest rates of medium-term erosion in 1989–2002. In the West marsh accretion zone, the first two satellite imagery EPR time-series are a poor match to the aerial photography EPR rates. By 2002–2014, however, the satellite imagery EPR and aerial photography EPR show closely mirrored accretion rates. At the West marsh, the medium-term accretion rates are increasing over time. As is evidenced by Fig. 5, Table D.1 and Fig. D.2 (Appendix D), the key EPR medium-term and WLR long-term average rate uncertainty for each salt marsh is greater for the satellite imagery than aerial photography time-series and the rate uncertainties reduce with improving spatial resolution. Compared to the EPR, the WLR rate uncertainty magnitude is lower and is not constant between the salt marsh patches, the West marsh has the greatest average rate uncertainty and the East marsh the lowest.

Overall, the satellite imagery WLR long-term shoreline rates-of-change and the satellite imagery EPR medium-term 2002–2014 rates-of-change are capable of mimicking the aerial photography rates well (Appendix D, Fig. D.2 and Fig. D.3). The satellite imagery rate-of-change accuracy, especially for the earlier medium-term EPR time-series, varies spatiotemporally (e.g. Appendix D, Fig. D.2). Both the aerial photography and the satellite imagery datasets demonstrate that the salt marsh system has active temporally non-linear erosion occurring at the toe of the South marsh and to a lesser extent along all the salt marsh shorelines that border the Faro Channel (Appendix D, Fig. D.3). Furthermore, the eastern flank of the West salt marsh is accreting at an increasing rate over time. There were also indications of gradual salt marsh expansion into the transitional zones bordering the sheltered channels within the study area (Appendix D, Fig. D.3).

Using the satellite imagery and aerial photography salt marsh areas, the medium- and long-term trends in salt marsh areas were calculated for the same time periods as for the shoreline trend analysis (Fig. 6). The satellite imagery area rates-of-change usually overestimate the aerial photography area erosion rates and underestimate the accretion rates (Fig. 6a and Fig. 6b). This error decreases as the average spatial resolution of the time-series improves, thus demonstrating the typical satellite imagery erosional bias observed in the shoreline rate analysis. The satellite imagery area rates are the least erosion biased in the West salt

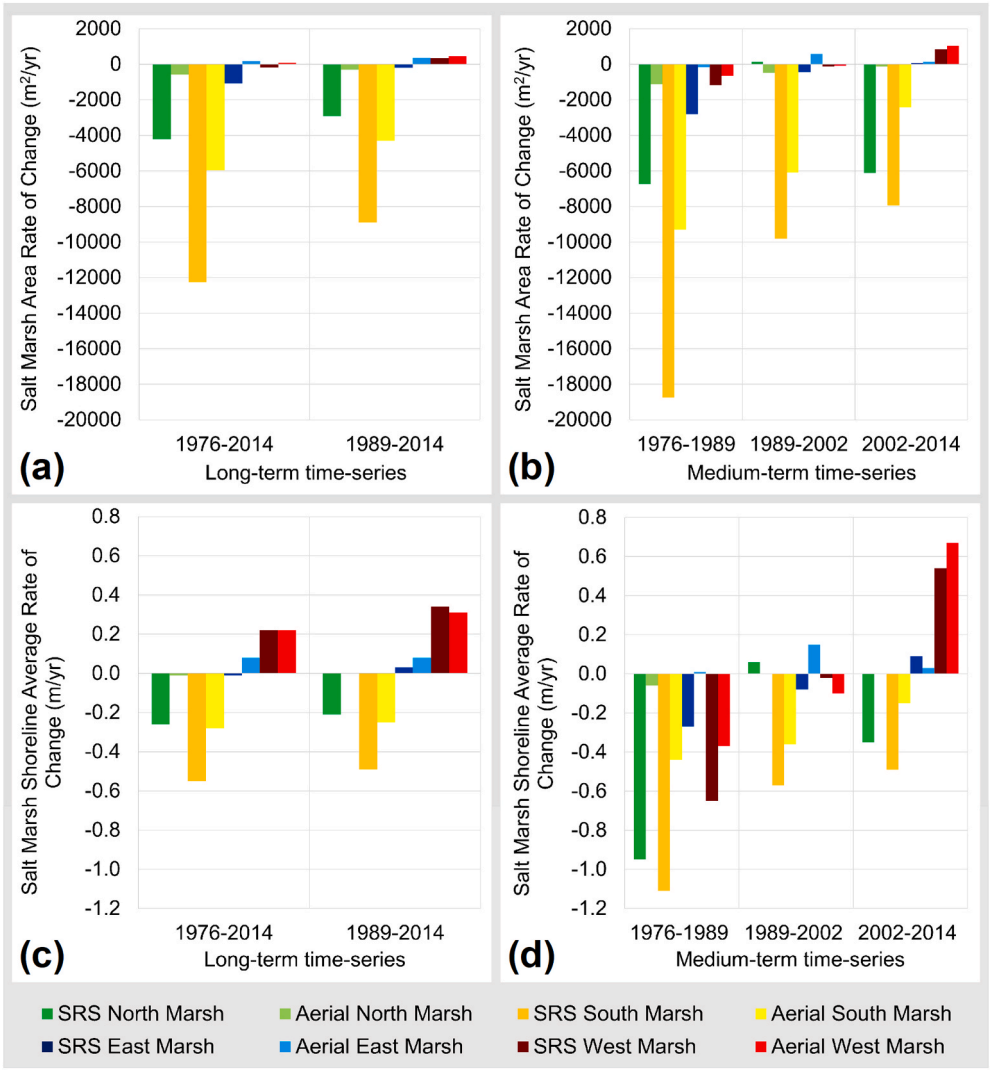

Fig. 6. Comparison of satellite remote sensing (SRS) and aerial photography (AP) salt marsh evolutionary trends over different time periods ordered by decreasing salt marsh size for the studied salt marsh patches, North, South, East and West: (a–b) surface area rates-of-change; (c–d) shoreline lateral position rates-of-change.

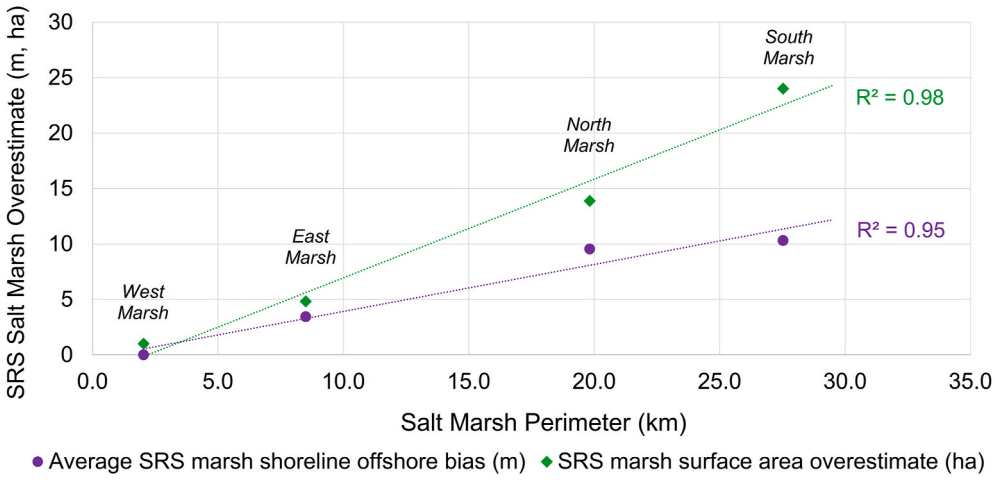

Fig. 7. The satellite remote sensing (SRS) 1976–2014 long-term time-series equivalent overestimate in surface area and average shoreline distance offshore plotted against aerial photography (AP) 2014 total salt marsh perimeter. The trendline coefficient of determination (R^2) has been included for each variable.

marsh and the most biased in the transitional zone rich South and North marshes. The comparative summary of the average shoreline rates-of-change is presented in Fig. 6c and Fig. 6d. Here the same trends outlined above are present, as both share the underlying accuracy limitations of the satellite remote sensing dataset. These two methods of measuring salt marsh extent change, however, appear to have different sensitivities to these limitations. The satellite imagery area rates are more consistently erosion biased than the satellite imagery shoreline average rates. Furthermore, the relative magnitude error between the satellite imagery and aerial photography in the area rates is higher and notably worse in the earlier time-series than for the shoreline rates. Hence, the satellite imagery area rates appear more vulnerable to the errors introduced by the inclusion of lower spatial resolution satellite imagery in the time-series than the satellite imagery shoreline rates (Fig. 4).

The satellite imagery 1976–2014 long-term time-series average shoreline and area rate-of-change errors were used to derive the time-series' equivalent average shoreline offshore bias and area overestimate for each of the salt marshes. While the satellite imagery 1976–2014 time-series equivalent shoreline average offshore bias for the North and the South marshes are similar, the time-series surface area overestimate error of the South marsh is almost double that of the similar sized North marsh (Fig. 7). The South marsh has significantly larger extents of transitional zones and in this environment the area evolution embeds higher uncertainty than the shoreline lateral evolution.

5. Discussion

5.1. Effects of salt marsh geometry and environmental characteristics on accuracy

In this study, the legacy of spatial resolution limitations in the satellite remote sensing data manifests usually as shoreline offshore bias. For the shoreline and area evolutionary trends, this transforms into faux erosion, which manifests as an overestimation of the aerial photography erosion and underestimation of the aerial photography accretion (Fig. 6). The faux erosion reduces through time as the accuracy of the satellite imagery shoreline delineation increases. The process is non-linear since there is faux erosion generated when the satellite imagery pixel size halves during 1976–1989 and halves anew during 1989–2002.

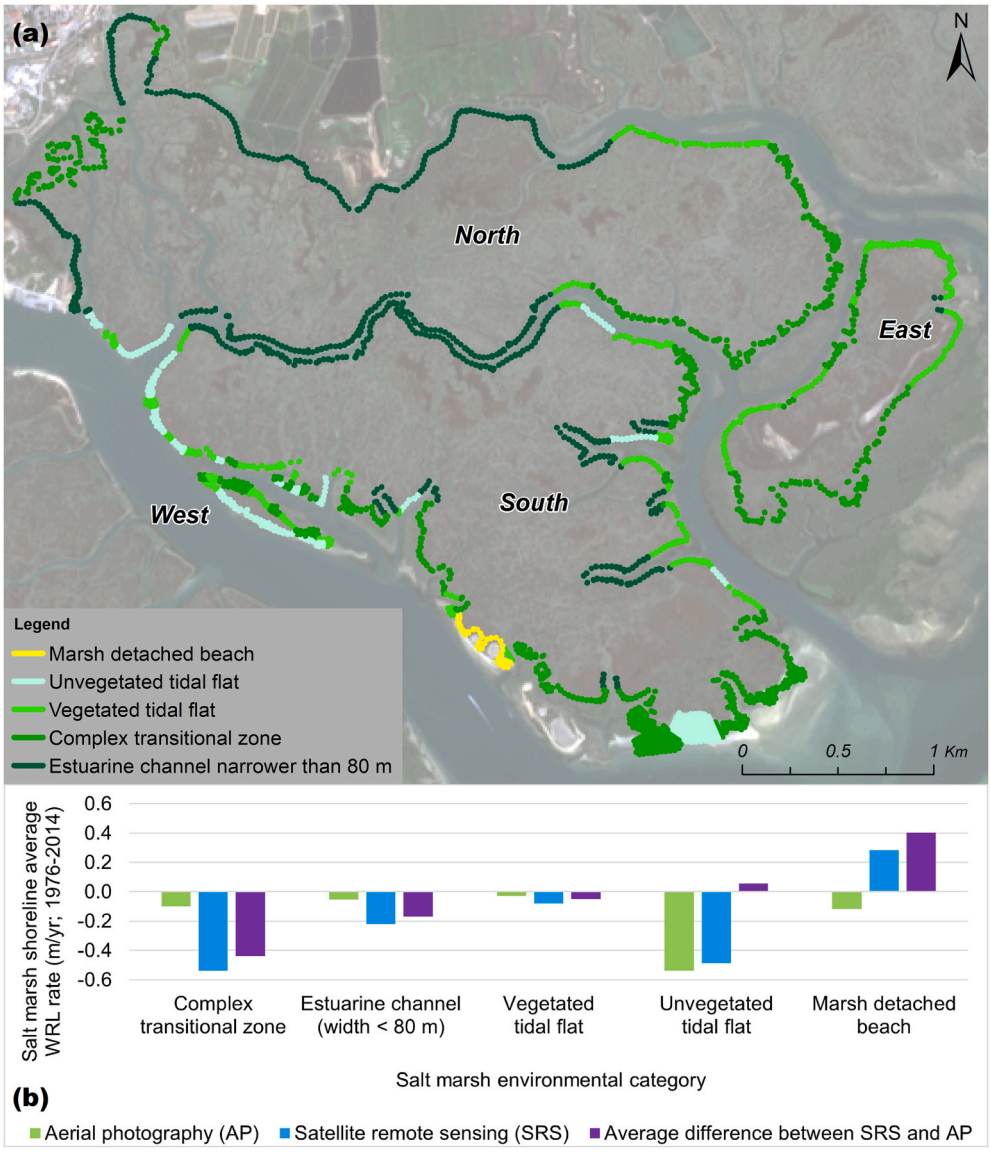

Fig. 8. (a) Map depicting the distribution of salt marsh shoreline environmental categories at the study site and (b) the aerial photography (AP) and satellite remote sensing (SRS) 1976–2014 time-series average salt marsh shoreline weighted linear regression (WLR) rates and error associated with each environmental category. ([Blount, 2020], contains modified Copernicus Sentinel-2B data [24-02-2020], processed by ESA).

Each of the salt marsh patches in this study site is unique in geometry, boundary conditions and the satellite remote sensing accuracy is influenced by these factors (e.g. Fig. 7). The feedback between fine-scale border morphologies and spatial resolution limits dictates the extremes of the satellite imagery salt marsh mapping errors (e.g. Figs. 4 and 8). The greatest source of inaccuracy is the transitional zones (Fig. 8b), the fragmented sections of salt marsh intermixed with vegetated tidal flats. In such cases, the uncertainties arise not only from the quality of the dataset, but also from the ecological and sedimentary dynamics of the environments themselves. In contrast to the marsh platform or dominantly estuarine (lagoon) zones, which are more stable in their environmental state, transitional zones represent a morphological state shifting between lower and higher levels of maturity or complexity. The latter raises the question about the influence of eco-morphological dynamics on the mapping of sedimentary environments, so far not extensively discussed in the scientific literature. In transitional zones there is mapping of the morphological process and not necessarily of the morphology. In the same way, tidal flats, which have a higher exposure to forcing mechanisms, can also be considered as transition zones when they shift between non-vegetated to vegetated environments (Fig. 8b).

To accurately capture the salt marsh shoreline in the transitional zone, the spatial resolution of the image needs to be close to the scale of the undulating shorelines and the colonising patches of salt marsh. Other boundary conditions such as marsh detached beaches and narrow estuarine channels can also degrade the satellite remote sensing shoreline accuracy (Fig. 8b), the former causing faux accretion while the latter faux erosion. However, unlike the more intricate transitional zones, their effect mostly dissipates once a 15 m spatial resolution is reached (e.g. Landsat-7 onwards) because at this scale the salt marsh shorelines in these environments can be reliably distinguished. A minor increase in spatial resolution from 15 m to 10 m was found to improve the transitional zone delineation accuracy, as demonstrated by the Landsat-8 shorelines being notably inland of transitional zone shorelines in comparison to the contemporaneous Sentinel-2 shorelines (Fig. 4 and Appendix D, Fig. D.1e). This aligns with the finding of Campbell and Wang (2020) that Sentinel-2 was necessary to improve the sensitivity of monitoring salt marsh fine-scale change.

The perimeter-area ratio has been proven useful as a landscape metric to measure salt marsh spatial patterns by Wu (2019). By employing this ratio in this study as well it was shown that for all the satellite sensors, there appears to be a directly proportional relationship between satellite imagery salt marsh area overestimation and the perimeter-area ratio (Fig. 3). Intricate transitional zones and fragmentation of the salt marsh result in a disproportionately large perimeter for a given salt marsh area, which is why the North marsh has a greater area than the South marsh yet a smaller perimeter (Fig. 2). Thus, the salt marsh perimeter-area ratio plotted against the total area can also prove useful as an indicator of the relative complexity of the salt marsh boundary conditions. If applied to a homogenous spatial resolution satellite imagery time-series, the perimeter-area ratio could be used as an indicator for a morphological trend such as the overall enlargement or fragmentation of the salt marsh platform.

The satellite remote sensing salt marsh area and shoreline rates-of-change have a similar pattern of inaccuracy across the salt marsh patches in the medium- and long-term time-series (Fig. 6). Nonetheless, the differences in the derivation and the core assumptions of the two methods of measuring salt marsh evolution mean that their application and interpretation in the context of ecosystem assessment differ. An advantage of the area method is that it does not require specific software to calculate the rates. However, this simplicity is a limit to the application of the area method for ecosystem management since its results are generalised trends. The shoreline method, in contrast, can be used to monitor salt marsh shoreline dynamics in detail on a transect-by-transect basis (e.g. Figs. 5 and 8). This enhances the potential of long-term time-series to elucidate the salt marsh system response to anthropogenic and natural drivers (Perennou et al., 2018; Vernberg, 1993).

The area rates of evolution are not furnished with rate statistics which can aid the interpretation of the significance and uncertainty of the trends at multi-levels of detail (Himmelstoss et al., 2018b). Nor does the area method allow shoreline uncertainty weighting to be applied to reduce satellite remote sensing erosion bias. These functionalities possessed by the shoreline method are vital for targeted salt marsh ecosystem monitoring. Taking these factors into account, the area method on its own does not provide the level of detail required for in-depth ecosystem-based management. Especially as the area method is slightly more sensitive than the shoreline method to the spatial resolution deficiencies in the open-source satellite datasets (Fig. 6). The area and shoreline methods, however, can be considered complementary to evaluate geomorphic trends and vulnerability in salt marshes and their ecosystem services. The area method supports ecosystem service assessments and evaluations (e.g. Muller-Karger et al., 2018; Sun et al., 2017) as well as stakeholder engagement (e.g. Burdon et al., 2019; Ryfield et al., 2019), while the shoreline rates provide detailed identification and monitoring of at-risk shorelines with complementary rate statistics and shoreline weightings to reduce implicit biases in long-term analyses (e.g. Fernandez-Nunez et al., 2019).

Likewise, the application of the WLR for long-term trends and EPR for medium-term can be complementary in the context of salt marsh monitoring through time. The satellite imagery WLR rates are more accurate than the EPR since the EPR results only incorporated two shorelines and there is no shoreline uncertainty weighting to reduce erosional bias. As a result of this, relying on the rates from a Landsat Multispectral Scanner (MSS) and a Landsat Thematic Mapper (TM) single-step medium-term time-series is not recommended. Similarly, reliance on results from a pairing of a Landsat TM with a pansharpened Landsat Enhanced Thematic Mapper Plus (ETM+) should also be made with caution. However, these issues aside, analysing the medium-term trends with the EPR method, in cases where there are less than three shorelines, can still help identify any temporal non-linearity masked by the WLR long-term trends (Ruggiero et al., 2013).

5.2. Salt marsh evolution in response to external drivers

The recent evolution (1976–2020) of the salt marsh shorelines was mostly induced by tidal channel dredging and inlet stabilisation (Carrasco et al., 2021). The observed minor erosion (up to −1.0 m/yr) on the shores of all the salt marshes bordering the Faro Channel (West, North and South marshes, Appendix D, Fig. D.3) is likely related to channel dredging and marine traffic, similar to elsewhere in the lagoon (Arnaud-Fassetta et al., 2006; Kombiadou et al., 2018). The South marsh has a northeast to a southwest gradient of increasing exposure to hydrodynamic forcing and its southern-most point is opposite the Faro-Olhão Inlet (Carrasco et al., 2021). In the 1976–2020 period, the South marsh exhibited a combination of static and accretional behaviour on its sheltered flanks, while being in erosion on the exposed flanks. The South mash has localised erosion opposite the Faro-Olhão Inlet with an average rate of −3.3 m/yr (Fig. 5e; Appendix D, Table D.1). The West marsh in comparison was dynamic along its entire perimeter with erosion on the flank adjacent to the Faro Channel and accretion on the side flanking the South marsh (Fig. 5e; Appendix D, Table D.1).

Overall, the satellite remote sensing long-term rates were relatively successful in capturing the dynamism of the aerial photography salt marsh shorelines and provided reasonable results. The satellite imagery rates for the shorelines with net long-term erosion or accretion greater than ± 0.4 m/yr were notably accurate (Appendix D, Fig. D.3). This enhanced accuracy is a result of dual aspects, the shoreline environmental category (Fig. 8) and that low rates of shoreline change are more vulnerable to the faux dynamism caused by the spatial resolution limits of the satellite imagery (Morton et al., 2004). In addition, by comparing the satellite imagery 1976–2020 shoreline rates with the salt marsh shoreline sinuosity and environmental category (Figs. 7 and 8) it was found that the most extreme rates of erosion and highest accuracy were

associated with smooth shorelines adjacent to unvegetated tidal flats, while areas of accretion were marked by the offshore expansion of complex transitional zones. These findings align with those of Leonardi et al. (2016), who found that shorelines with the greatest erosion rates were less intricate, and Elsey-Quirk et al. (2019) who noted a connection between salt marsh morphodynamics and vegetation patterns.

5.3. Satellite remote sensing overall performance

In literature, medium to high spatial resolution multispectral data is an accepted alternative to hyperspectral high-resolution data (Belluco et al., 2006; Klemas, 2013a; Young et al., 2017), unless salt marsh vegetation detailed analysis is required (Guo et al., 2017; Müllerová et al., 2017; Silvestri et al., 2003). There is a general lack of salt marsh studies using long-term time-series that reach four decades, which reduces the meaningfulness of any morphological, socio-economic and ecosystem service analysis (Barbosa et al., 2015; Carrasco, 2019). Among other things, long-term trends can help distinguish salt marsh system responses to change and forms a reference baseline to contextualise medium-to short-term times-series (Moffett et al., 2015; Vernberg, 1993). Thus, the pooling of all the open-source satellite remote sensing data available to form long-term time-series used in this study is advantageous and valid.

In other studies, the paucity of suitable satellite remote sensing images and sensor reflectance conversion algorithms, as well as the low resolution of the early years of the Landsat programme, frequently limits the length of the time-series (e.g. Campbell and Wang, 2020; Laengner et al., 2019; Vogelmann et al., 2016). Usually, a minimum of 30 m spatial resolution was used to map coastal wetlands and the MSS data was disqualified from the analyses (e.g. Bortels et al., 2011; Rebelo et al., 2017; Turpie et al., 2015). The few studies that have used Landsat MSS data for salt marshes have done so with a significant sacrifice of spatial accuracy or have fused it with supplementary data (Jefferies et al., 2006; Niu et al., 2012; Sivakumar and Ghosh, 2016). These studies neither incorporate all Landsat sensors nor are quadridecadal in duration. Using the method employed in this study, it was shown that the inclusion of the Landsat MSS data allowed eco-geomorphologically valuable long-term trends to be derived and the inaccuracies due to the inclusion of this data can be at least partially compensated for by using the WLR method to calculate shoreline rates-of-change. In addition, the mapping accuracy and uncertainty assessment of satellite remote sensing wetland maps and long-term monitoring are needed but lacking (Perennou et al., 2018; Pham et al., 2019; Reschke and Hüttich, 2014). The satellite remote sensing tool investigated in this study fulfils an element of that knowledge gap. Furthermore, since the satellite remote sensing method tested quantifies the associated accuracies, it can support more accurate salt marsh ecosystems valuation (Barbosa et al., 2015).

During the literature review, no equivalent studies were found that quantified the relative accuracy of aerial photography and open-source optical satellite remote sensing for salt marsh shoreline delineation and monitoring, even at less than a quadridecadal duration. However, although not directly comparable, studies using satellite imagery to map salt marshes by incorporating external data sets, indexes and classification methods have achieved classification accuracies of over 90% (e.g. Laengner et al., 2019; Lopes et al., 2020; Mao et al., 2020). Some inaccuracy causing factors encountered in this study were also noted by other remote sensing studies of salt marshes. These include difficulties distinguishing the land border (Laengner et al., 2019); salt marsh area overestimation (Belluco et al., 2006; Rebelo et al., 2017); interference of surface sediment spectral properties with that of salt marsh vegetation (Belluco et al., 2006; Silvestri et al., 2003); issues detecting salt marsh patches in the transitional zone (Arnaud-Fassetta et al., 2006; Bortels et al., 2011; Kelleway et al., 2009); accuracy differences between different spatial resolutions adding error to time-series (Guo et al., 2017; Rebelo et al., 2017); longer perimeters resulting in lower levels of accuracy (Fisher et al., 2016) and; surface reflectance pixel mixing (Bortels et al., 2011; Klemas, 2013b; Reschke and Hüttich, 2014). Thus, the sources of error encountered in this study are generalised in the research field and not specific limitations of the satellite remote sensing method proposed.

5.4. Future research directions

The study limitations are (a) the Landsat pansharpening bands and the Landsat MSS sensor bands were not yet available as a Level 2 product and this may be a source of inaccuracy in the results; (b) the oldest sensors within the Landsat programme have lower spatial resolution and thus introduce additional error, although their inclusion is balanced by the need to derive long-term trends; (c) the seasonality in salt marsh vegetation spectral signatures may affect the accuracy of the method; (d) the method is limited in its ability to monitor gradual change at small scales due to lack of temporal density, spatial resolution and the masking effects of faux shoreline change (Vogelmann et al., 2016); (e) the satellite remote sensing salt marsh mapping accuracy assessment that has been undertaken in this study is made with reference to an alternative remote sensing method, aerial photography, and not ground truth data.

There are future research directions that could mitigate these current limitations by expanding the scope and improving the accuracy of long-term time-series using open-source optical satellite remote sensing data. From a technical perspective, trialling the fusion of synthetic aperture radar (SAR) and multispectral data in a long-term time-series is a promising technique that should be explored (Pham et al., 2019). In addition, coupling the satellite remote sensing method with additional data in modelling environments could enhance the ability to link drivers to salt marsh response and ecosystem service availability (Barbosa et al., 2015). Furthermore, spatial pattern metrics have been shown to introduce fewer biases than total areas in salt marsh remote sensing studies (Wu, 2019). Hence, the integration of a fractal index (e.g. Carrasco et al., 2021; Dubuc et al., 1989; Rebelo et al., 2017) is recommended as a measure for transitional zones as well as a geomorphic indicator of the degradation state of salt marshes (Leonardi et al., 2016) and intertidal ecosystem fragmentation (Cunha et al., 2005). In addition, a broad range of salt marshes in distinct environmental conditions need to be analysed to further clarify how specific salt marsh characteristics and local climate affects the accuracy of the satellite remote sensing results. This would consolidate the applicability limits of the method on a global scale. The collection of further salt marsh case studies would also define the apparent directly proportional relationship between salt marsh perimeter and the equivalent surface area and average salt marsh shoreline offshore biases in long-term time-series (Fig. 7). If such a relationship could be established, predictions could be made of the inherent biases in any satellite remote sensing salt marsh analysis based on its perimeter. This could in turn be used to make predictive corrections to the satellite remote sensing results and thus improve the accuracy of the method.

6. Conclusions

This study demonstrated that the open-source multispectral satellite remote sensing archive can be used to map salt marsh extents and monitor their long-term shoreline dynamics at a level of accuracy appropriate for the many ecological assessment and management applications that do not require fine-scale detail. In the central section of the Ria Formosa coastal lagoon during 1976–2020, there was a net loss of salt marsh habitat, with the maximum rates of salt marsh erosion being concentrated opposite the Faro-Olhão tidal Inlet.

The sensitive accuracy analysis found that the satellite remote sensing salt marsh shoreline's positional accuracy is a function of sensor characteristics as well as the salt marsh geometry, environment and temporal dynamism. The aerial photography salt marsh areas and perimeters were respectively overestimated and underestimated by the satellite remote sensing results. The Landsat-8 shorelines were slightly

less accurate and on average 1.8 m inland of the coincident Sentinel-2 shorelines. The higher spatial resolution of the latter sensor resulted in slightly larger areas and longer perimeters.

The increasing spatial resolution over time resulted in temporally dynamic shoreline offshore bias and thus faux erosion in the satellite imagery time-series. Furthermore, the shoreline and area inaccuracies of the satellite remote sensing method were found to be a cumulative function of salt marsh perimeter. The satellite imagery shorelines are least accurate when there are complex boundary conditions that require a higher spatial resolution to delineate. The intricate shorelines of the transitional zones were the focal points of error for all the satellite imagery shorelines and these amplified the offshore bias and faux erosion present in the time-series. The outcome of the analysis points to an interesting aspect of mapping these tidally dominated environments. Apart from being able to examine the long-term development of each morphology individually, it is also possible to explore the transitional processes between different states of eco-geomorphological complexity.

Overall, the satellite remote sensing methodology evaluated in this study is suitable as a tool for salt marsh shoreline mapping and monitoring in a research and operational coastal management context, as long as due regard is given to its specific limitations. Although not as accurate as the aerial photography data, the satellite remote sensing data returns reasonable estimates and can approximate long-term shoreline dynamics of interest in a cost-effective way.

Author statement

Tegan R. Blount: Conceptualization, Methodology, Validation, Formal analysis, Investigation, Data curation, Writing—original draft preparation, Visualization, Project administration and Funding acquisition. **A. Rita Carrasco**: Conceptualization, Methodology, Resources, Writing—review and editing; Supervision and Funding acquisition. **Sónia Cristina**: Conceptualization, Methodology, Resources, Writing—review and editing; Supervision and Funding acquisition. **Sonia Silvestri**: Resources, Writing—review and editing and Supervision.

Declaration of competing interest

The authors declare that they have no known competing financial interests or personal relationships that could have appeared to influence the work reported in this paper.

Acknowledgements

This work and Tegan R. Blount were funded by the Murray Foundation supporting student research, https://www.murrayfoundation.eu, [grant number 01.11.2020] and the European Commission under the Erasmus Mundus Joint Master Degree Programme in Water and Coastal Management [grant number 586596-EPP-1-2017-1-IT-EPPKA1-JMD-MOB]. Sónia Cristina was supported by Fundação para a Ciência e a Tecnologia, I.P., Portugal [grant number CEECIND/01635/2017]. A. Rita Carrasco was funded by Fundação para a Ciência e a Tecnologia, Portugal [grant number DL 57/2016/CP1361/CT0002]. The authors would like to acknowledge CIMA - Centre for Marine and Environmental Research (UID/00350/2020CIMA); Faculty of Marine and Environmental Sciences (CASEM) University of Cadiz; USGS Landsat Archive; Copernicus Open Access Hub; and the two anonymous reviewers of this article.

Appendix A

A.1 Salt Marsh Morphology and Vegetation

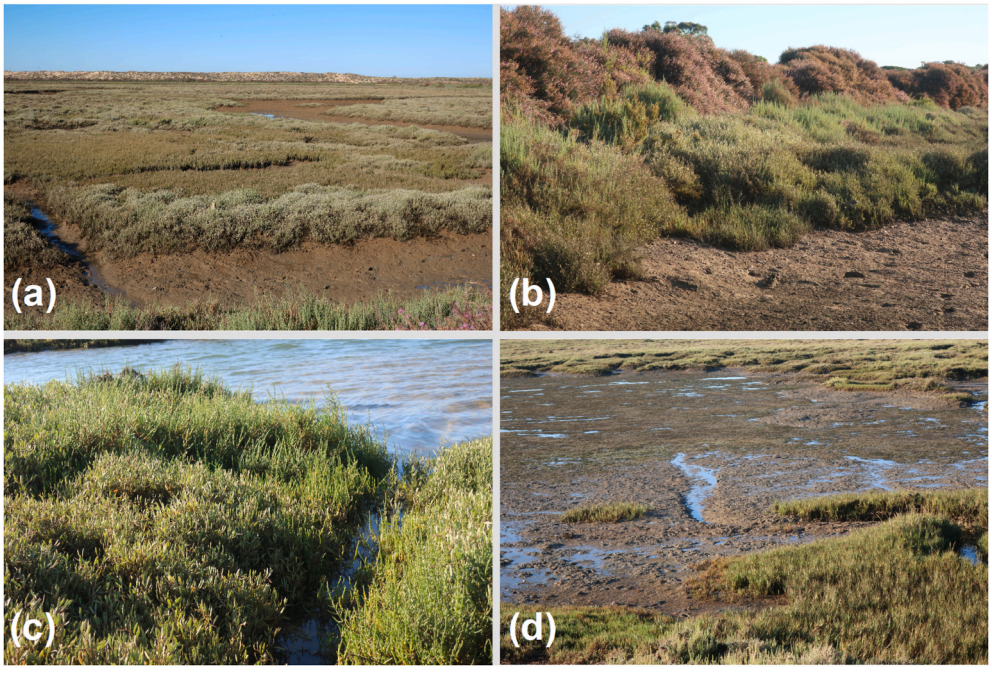

Fig. A.1. (a) Salt marsh platform above the tidal flats with halophytic vegetation displaying a mosaic zonation pattern [Blount, 19-06-2020]; (b) salt marsh vegetation showing vertical zonation [Blount, 29-06-2020]; (c) middle to low salt marsh halophytes *Sarcocornia perennis* and *Halimione portulacoides* [Blount, 11-06-2020]; (d) *Spartina maritima* and *Zostera noltii* colonising the low elevation transitional zone between salt marsh and tidal flats [Blount, 29-06-2020].

Appendix B

B.1 Remote Sensing and Field Datasets

Table B.1
Attributes of the satellite remote sensing and aerial photography datasets used in the study.

Year	Type	Sensing Date	Resolution (m)	No. Bands
1976	Aerial Photograph	31 August	0.73	1
	Landsat-1 MSS Image	29 March	57.00*	4
1989	Aerial Photograph	4 May	0.38	1
	Landsat-5 TM Image	23 March	30.00	7
2002	Aerial Orthophotograph	June**	0.70	3
	Landsat-7 ETM + Image	15 February	15.00***	8
2014	Aerial Orthophotograph	22 October	0.15	4
	Landsat-8 OLI Image	31 May	15.00***	8
2016	Landsat-8 OLI Image	08 August	15.00***	8
	Sentinal-2A MSI Image	08 August	10.00	10
2018	Landsat-8 OLI Image	02 January	15.00***	8
	Sentinal-2B MSI Image	02 January	10.00	10
2020	Landsat-8 OLI Image	25 February	15.00***	8
	Sentinal-2B MSI Image	24 February	10.00	10

*Original spatial resolution 80 m up sampled to 57 m prior to public distribution (Read et al., 2020; Young et al., 2017).
**Missing date metadata.
***Pansharpening applied to increase spatial resolution from 30 m to 15 m.

Field observations included three GPS topographic transects, collected on 13 January 2017, that intersect the salt marsh shoreline in the study area. These profiles are named South Salt Marsh Profile 1 (S1), South Salt Marsh Profile 2 (S2) and North Salt Marsh Profile 1 (N1). The elevation profile along each transect and the sampling points were obtained by using a Real-Time Kinematic Differential Global Positioning System (RTK-GPS, Trimble R6) sampling at 1 Hz. The elevation units were in metres relative to mean sea level (MSL). On average the three GPS transects had 30 points in each profile, N1 had fewer points due to difficulties traversing the salt marsh. The measurements were taken at a mean distance of ~1 m and the vertical accuracy was in the order of centimetres. These transects were taken as part of a study which aimed to validate the salt marsh zonation, especially in the transition zone between tidal flat and low salt marsh, and to also track the bed slope transitions.

B.2 Image Selection Criteria and Processing

The selection of the time-series years was dictated by the need for the simultaneous availability of both an aerial photography survey and a suitable satellite remote sensing image. Considering this requirement, the years chosen for the aerial photography and satellite remote sensing comparison were 1976, 1989, 2002 and 2014. There were no aerial photography datasets available beyond 2014 and the Sentinel-2 programme did not launch until 2015. Therefore, the comparability and complementary potential of Sentinal-2 was gauged against Landsat-8 in 2016, 2018 and 2020, which also allowed the satellite remote sensing time-series to be extended to 44 years. SRS atmospherically corrected data was preferred as it provides an accurate and stable surface reflectance record, as recommended for a time-series analysis (Roy et al., 2014; Vogelmann et al., 2016). Furthermore, this analysis-ready data was the most appropriate choice for this study since the study objectives require standardised, established open-source globally available satellite remote sensing images that are not time-consuming nor require expertise to process.

The satellite remote sensing image selection was decided by cloud coverage, tidal level and the season. The tidal stage response can be variable across salt marsh systems, and it has been demonstrated that the accuracy of long-term trends in salt marshes can be enhanced by tidal filtering of images (Campbell and Wang, 2018, 2020). Thus, only images at a low tidal stage were considered to avoid inundation induced salt marsh boundary delineation errors. There was only one suitable satellite remote sensing image available for 1976 and since there is seasonal variation in salt marsh vegetation spectral signatures (Gao and Zhang, 2006), the remaining selection of satellite remote sensing images for the later years were filtered to be from a similar time of year as possible. In the case of the Sentinel-2 and Landsat-8 pairs of satellite remote sensing images, they were selected to also be coincident or at least within 24 h of each other to enhance comparability.

The remote sensing images were prepared and analysed in ArcGIS Desktop 10.5 (ESRI, 2016) and Sentinel Application Platform (SNAP) v7.0.3 (European Space Agency ESA, 2019). The 1976 and 1989 aerial photography rasters were georectified with a method analogous to Amado (2019) and Kombiadou et al. (2019). The surface reflectance correction of the 2016 and 2018 Sentinel-2 images was undertaken with the Sen2Cor 280 extension in SNAP, as for these dates Level 2A data was not available on the open-access hub. For optical sensors with a panchromatic band, pansharpening - an established technique for increasing the spatial resolution of multispectral bands (Meng et al., 2019; Vivone et al., 2015) - was applied as per the context adaptive Gram-Schmidt (GSA) method. A component substitution method, GSA is a robust choice for this study as it is less vulnerable to aliasing and misregistration between the panchromatic band and multispectral bands and is a less computationally intense method (Duran et al., 2017; Meng et al., 2019; Vivone et al., 2015). In addition, the GSA technique has been demonstrated to be suitable for Landsat-8 Operational Land Imager (OLI) applications and has comparatively low spatial distortion (Vivone et al., 2015; Zhang and Roy, 2016).

Appendix C

C.1 Salt Marsh Shoreline Accuracy and Validation

The average root-mean-square (RMS) values for the georeferenced aerial photographs of 1976 and 1989 were 0.9 m and 0.5 m respectively. The shoreline location uncertainties assigned to each shoreline as part of the Digital Shoreline Analysis System (DSAS) analysis were between 0.4 m (2014) and 3.1 m (1976) for the aerial photography data while for the satellite remote sensing data these ranged between 15 m (Sentinal-2B 2020) to 69 m (Landsat-1 1976). Both the RMS and shoreline location uncertainties are in the horizontal plane.

During validation, the topographical transects from fieldwork data collection (not published) were overlaid with the delineated satellite remote

sensing and aerial photography shorelines and the horizontal and vertical coordinates of these shorelines on the transect profiles was calculated. As there was no field data available to validate the horizontal position directly and these transects are from sections of salt marsh that have shown minimal lateral migration over the last four decades (Fig. 5a; Carrasco et al., 2021), the remote sensing shoreline elevation ranges derived from the transects were compared with elevation ranges for lower-middle salt marsh in literature (Table C.1). The remote sensing shoreline elevations from the profiles were generally within the lower-middle salt marsh ranges identified in Arnaud-Fassetta et al. (2006), Sun et al. (2018) and Andrade (1990) (0.0–0.4/2.0 m, MSL). The lower bound of the range in Costa et al. (1996) and Bettencourt (1994) (0.5–1.0 m, MSL) was reflective of the upper-middle salt marsh bionomic range of Arnaud-Fassetta et al. (2006) and thus the elevation ranges from the remote sensing shorelines were consistently lower than these. Overall, the elevation ranges derived for the remote sensing shorelines from the field profiles are within the expected elevation range for a lower-middle salt marsh boundary in literature.

Table C.1
The elevation ranges (in metres above Mean Sea Level, MSL) of the delineated shorelines on the topographic transects used for shoreline validation (AP- Aerial Photograph; SRS - Satellite Remote Sensing, S2B – Sentinel 2B; L8 – Landsat-8; L7 – Lansat-7; L5 – Landsat-5; L1 – Landsat-1)

Salt Marsh Shoreline	SRS S2B 2020	SRS L8 2020	AP 2014	SRS L8 2014	AP 2002	SRS L7 2002	AP 1989	SRS L5 1989	AP 1976	SRS L1 1976
Lower-middle salt marsh range (m, MSL)	[-0.30 to 0.14]	[0.08 to 0.50]	[0.15 to 0.31]	[0.08 to 0.23]	[0.16 to 0.30]	[-0.34 to 0.62]	[0.25 to 0.48]	[-0.29 to 0.32]	[0.26 to 0.51]	[0.17 to 0.42]

As a further validation, the transect profiles and shoreline points were overlaid with bionomic elevation ranges from a study of the Ria Formosa salt marshes (Arnaud-Fassetta et al., 2006). Generally, the aerial photography 2014 shorelines were approximately at MSL, the central part of the lower-middle salt marsh range (Fig. C.1). The remaining salt marsh shorelines spanned the whole lower-middle salt marsh range, sometimes extending to the upper-middle or lower salt marsh ranges in profiles N1 and S2. Compared to the Landsat-8 2020 shoreline, the Sentinel-2B 2020 shoreline consistently favoured the low salt marsh zone and the satellite remote sensing shorelines are on average more offshore than their aerial photography counterparts.

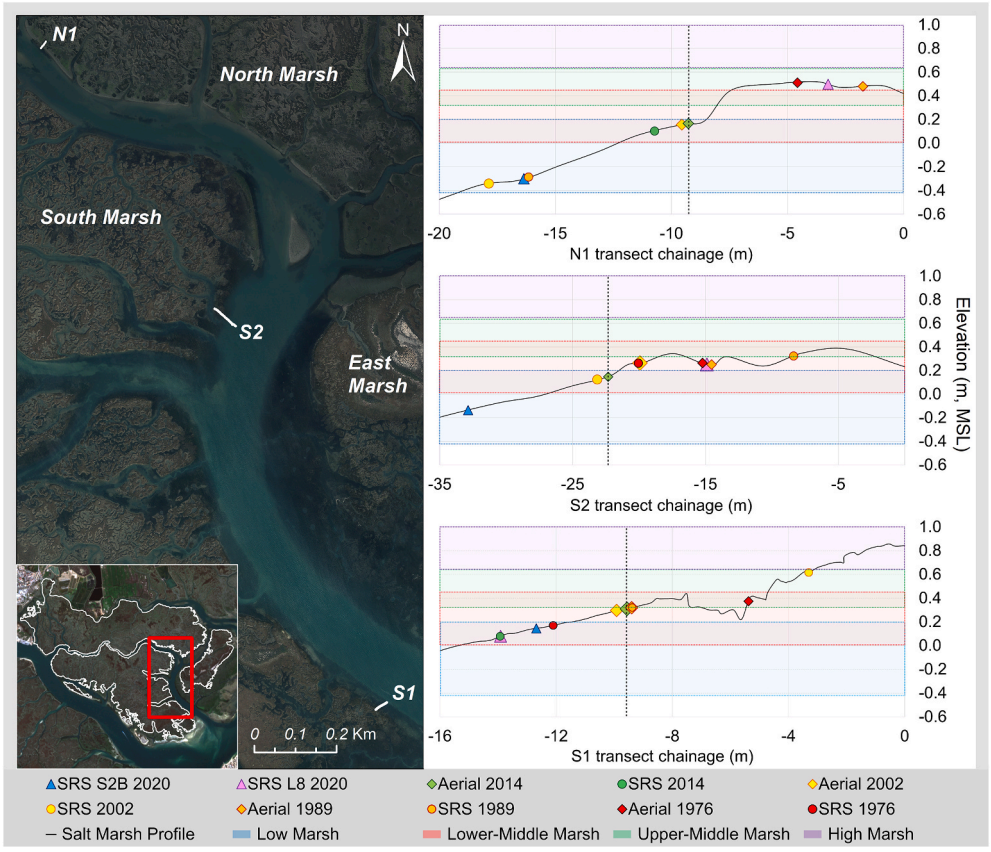

Fig. C.1. Location of field topographical transects and the satellite remote sensing (SRS) and aerial photography (AP) shoreline positions and salt marsh bionomic ranges on the field topographic transects N1, S2 and S1. The approximate 2017 shoreline position is indicated by the vertical dotted line intersecting each profile. (The main image contains RGB mosaic of the 2014 aerial orthophotos; the overview image [Blount, 2020], contains modified Copernicus Sentinel-2B Level 2A data [24-02-2020]).

As a result of its high spatial resolution and temporal closeness, the aerial photography 2014 shoreline is a reliable indication of the actual 2017 salt marsh shoreline position on the transect profiles. Given the lateral stability of these shorelines over the last decades (Fig. 5a; Carrasco et al., 2021), the aerial 2014 shoreline can also approximately indicate the lateral inaccuracy of the other remotely sensed shorelines. The results validate the vertical and horizontal position of the 2014 aerial shoreline and highlight variable degrees of error in the lateral position of the other remote sensing shorelines.

Appendix D

D.1 Salt Marsh Shoreline Analysis

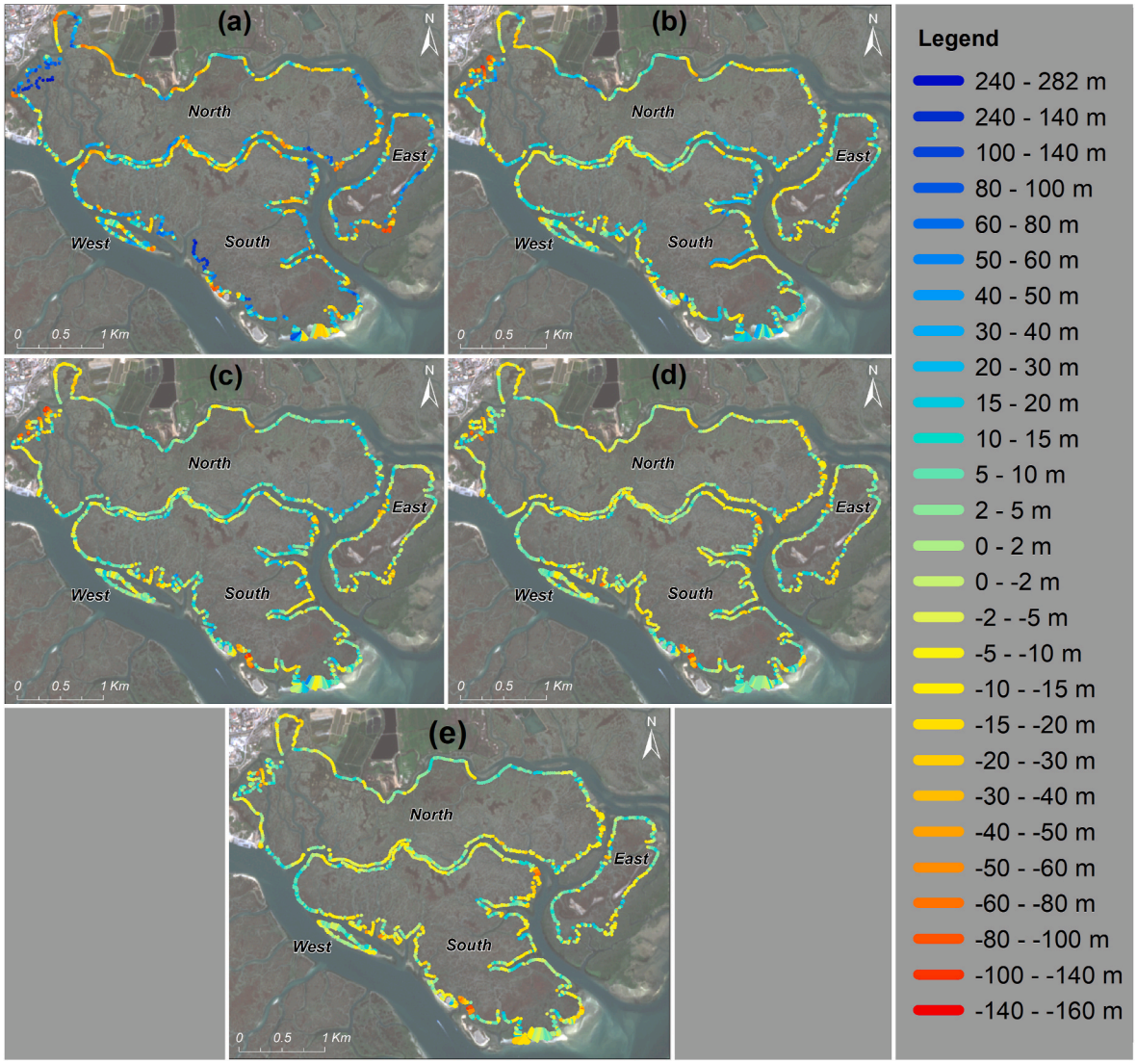

Fig. D.1. Maps depicting the distance (m) of: (a) the 1976 Landsat-1 shoreline relative to the aerial photography (AP) 1976 shoreline; (b) the 1989 Landsat-5 shoreline relative to the AP 1989 shoreline; (c) the 2002 Landsat-7 shoreline relative to the AP 2002 shoreline; (d) The 2014 Landsat-8 shoreline relative to the AP 2014 shoreline and (e) the 2020 Landsat-8 shoreline relative to the 2020 Sentinel-2B shoreline. ([Blount, 2020], contains modified Copernicus Sentinel-2B data [24-02-2020], processed by ESA).

Table D.1
Summary of the satellite remote sensing (SRS) and aerial photography (AP) salt marsh shoreline Weighted Linear Regression (WLR; long-term) and End Point Rate (EPR; medium-term) results from the shoreline rate analysis.

Salt Marsh Area	Time Period	Data Source	Average Rate (m/yr)	Rate Uncertainty (m/yr)	Maximum Erosion Rate (m/yr)	Average Erosion Rate (m/yr)	Maximum Accretion Rate (m/yr)	Average Accretion Rate (m/yr)
Long-term Weighted Linear Regression Shoreline Rates								
North	1976–2014	AP	−0.01	±0.02	−0.81	−0.12	1.64	0.16
		SRS	−0.26	±0.51	−4.15	−0.59	3.57	0.48
	1989–2014	AP	0.00	±0.04	−0.90	−0.13	1.79	0.18
		SRS	−0.21	±0.75	−2.41	−0.62	5.41	0.64
	1976–2020	SRS	−0.05	±0.27	−2.68	−0.42	3.97	0.44
East	1976–2014	AP	0.08	±0.03	−0.74	−0.14	1.16	0.15
		SRS	−0.01	±0.24	−2.03	−0.42	1.51	0.39
	1989–2014	AP	0.08	±0.04	−0.79	−0.14	1.25	0.17
		SRS	0.03	±0.52	−1.89	−0.43	1.85	0.41
	1976–2020	SRS	0.09	±0.16	−0.95	−0.31	1.16	0.39

(*continued on next page*)

Table D.1 (*continued*)

Salt Marsh Area	Time Period	Data Source	Average Rate (m/yr)	Rate Uncertainty (m/yr)	Maximum Erosion Rate (m/yr)	Average Erosion Rate (m/yr)	Maximum Accretion Rate (m/yr)	Average Accretion Rate (m/yr)
South	1976–2014	AP	−0.28	±0.08	−5.19	−0.44	1.60	0.13
		SRS	−0.55	±0.35	−4.93	−0.90	1.73	0.37
	1989–2014	AP	−0.25	±0.13	−5.81	−0.45	1.99	0.16
		SRS	−0.49	±0.50	−5.60	−0.90	2.00	0.38
	1976–2020	SRS	−0.46	±0.18	−6.38	−0.8	1.22	0.29
West	1976–2014	AP	0.22	±0.18	−1.27	−0.33	1.76	0.56
		SRS	0.22	±0.48	−0.89	−0.33	1.82	0.63
	1989–2014	AP	0.31	±0.39	−1.26	−0.37	2.34	0.65
		SRS	0.34	±1.07	−0.71	−0.26	2.26	0.70
	1976–2020	SRS	0.26	±0.26	−0.78	−0.35	1.73	0.66
Medium-term End Point Shoreline Rates								
North	1976–1989	AP	−0.06	±0.27	−1.60	−0.26	2.15	0.21
		SRS	−0.95	±5.86	−21.18	−3.34	6.95	2.06
	1989–2002	AP	0.00	±0.20	−2.19	−0.18	3.45	0.20
		SRS	0.06	±2.75	−6.02	−1.07	7.38	1.13
	2002–2014	AP	0.00	±0.17	−1.55	−0.17	2.04	0.24
		SRS	−0.35	±1.83	−5.07	−0.98	10.02	1.02
East	1976–1989	AP	0.01	±0.27	−1.61	−0.37	2.76	0.27
		SRS	−0.27	±5.86	−5.61	−1.89	8.44	2.00
	1989–2002	AP	0.15	±0.20	−1.10	−0.18	2.66	0.31
		SRS	−0.08	±2.75	−3.05	−0.92	2.70	0.97
	2002–2014	AP	0.03	±0.17	−0.96	−0.16	1.83	0.16
		SRS	0.09	±1.83	−3.31	−0.67	3.88	0.76
South	1976–1989	AP	−0.44	±0.27	−9.89	−0.80	1.28	0.24
		SRS	−1.11	±5.86	−19.29	−3.04	6.78	1.88
	1989–2002	AP	−0.36	±0.20	−9.01	−0.77	4.29	0.31
		SRS	−0.57	±2.75	−9.99	−1.71	5.66	0.94
	2002–2014	AP	−0.15	±0.17	−6.15	−0.32	2.47	0.17
		SRS	−0.49	±1.83	−6.46	−1.09	2.14	0.55
West	1976–1989	AP	−0.37	±0.27	−2.02	−0.71	1.54	0.52
		SRS	−0.65	±5.86	−4.88	−1.60	5.55	1.43
	1989–2002	AP	−0.10	±0.20	−1.49	−0.51	1.86	0.42
		SRS	−0.02	±2.75	−1.98	−0.70	3.09	1.01
	2002–2014	AP	0.67	±0.17	−1.07	−0.43	3.88	1.17
		SRS	0.54	±1.83	−1.38	−0.59	3.44	1.20

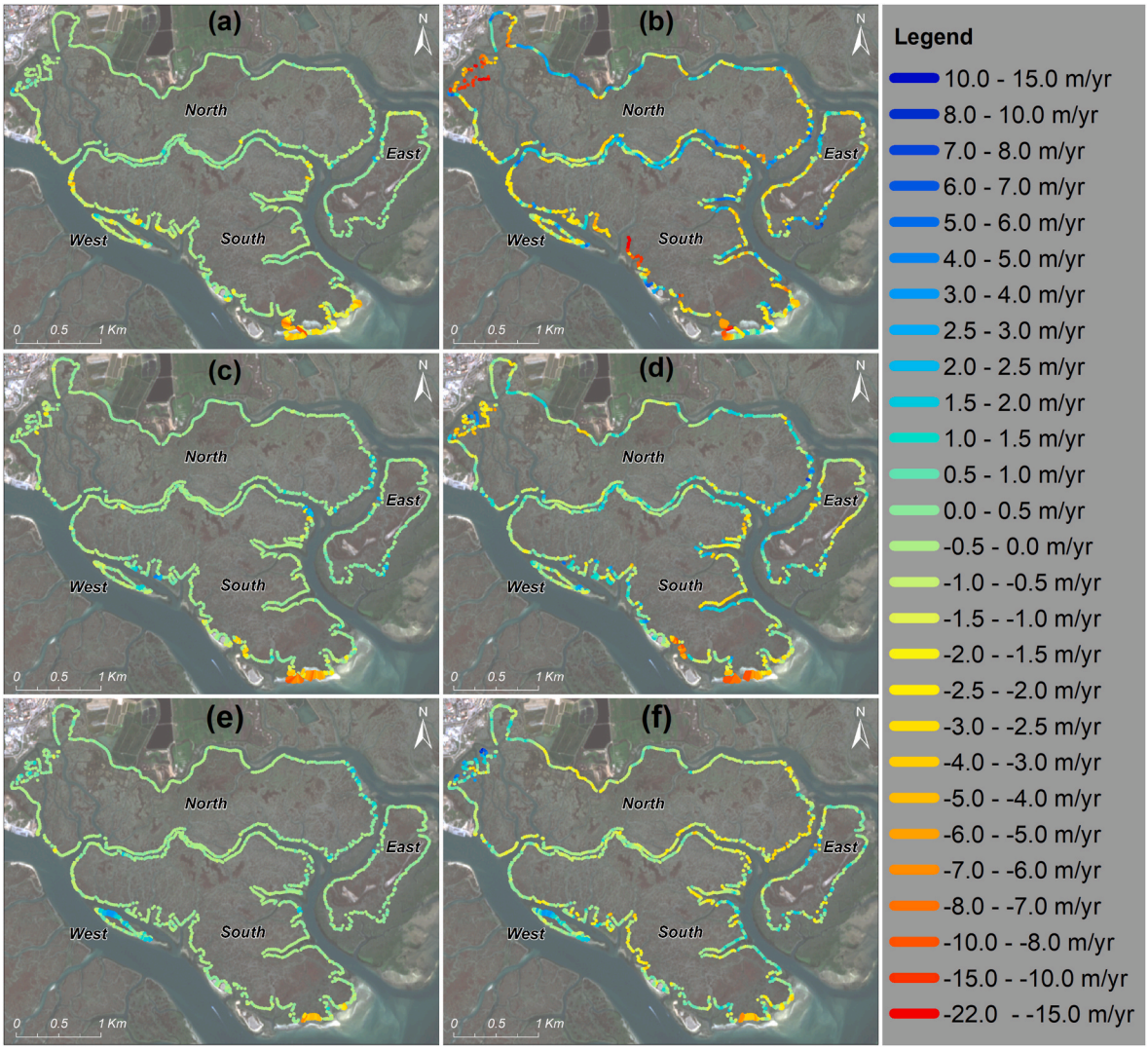

Fig. D.2. Maps depicting salt marsh shoreline End Point Rates (EPR) (m/yr) for: (a) aerial photography (AP) 1976–1989; (b) Satellite remote sensing (SRS) 1976–1989; (c) AP 1989–2002; (d) SRS 1989–2002; (e) AP 2002–2014; and (f) SRS 2002–2014. ([Blount, 2020], contains modified Copernicus Sentinel-2B data [24-02-2020], processed by ESA).

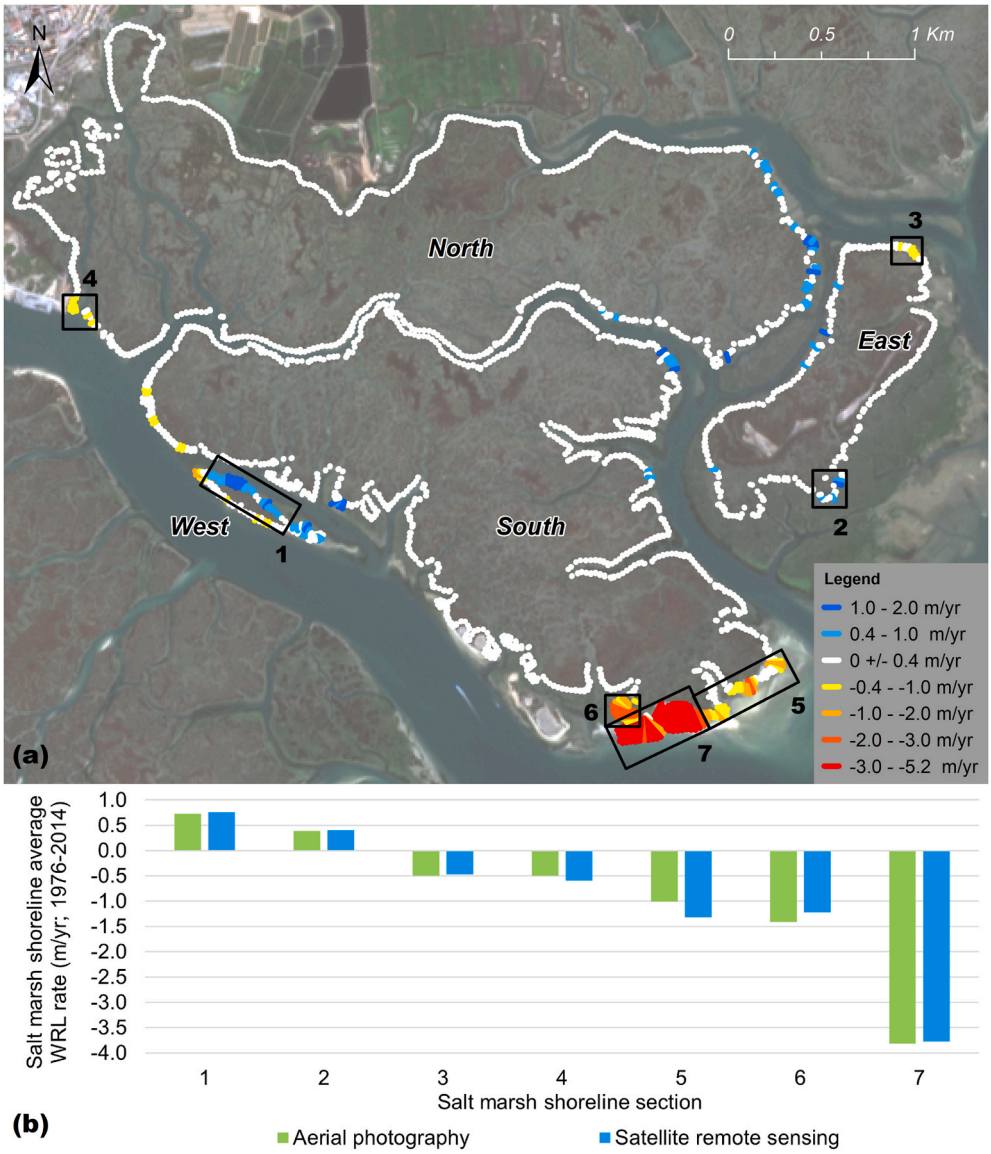

Fig. D.3. (a) Map highlighting the salt marsh shorelines where the aerial photography (AP) weighted linear regression (WRL) rates-of-change (m/yr) for the 1976–2014 time-series are more than ± 0.4 m/yr; (b) graph showing the relative accuracy of the average satellite remote sensing (SRS) and AP 1976–2014 WRL shoreline rates-of-change for specific sections of salt marsh shoreline. ([Blount, 2020], contains modified Copernicus Sentinel-2B data [24-02-2020], processed by ESA).

Appendix E. Supplementary data

Supplementary data to this article can be found online at https://doi.org/10.1016/j.ecss.2021.107664.

References

Amado, P.M.D.S.V., 2019. Salt Marsh Response to Changing Hydrodynamics: the Case of Ancão Inlet Migration (Ria Formosa Coastal Lagoon). Universidade do Algarve. http://hdl.handle.net/10400.1/13895.

Andrade, C., 1990. O Ambiente Barreira da Ria Formosa. University of Lisboa, Algarve-Portugal.

Andrade, C., Freitas, M.C., Moreno, J., Craveiro, S.C., 2004. Stratigraphical evidence of Late Holocene barrier breaching and extreme storms in lagoonal sediments of Ria Formosa, Algarve, Portugal. Mar. Geol. 210, 339–362. https://doi.org/10.1016/j.margeo.2004.05.016.

Arnaud-Fassetta, G., Bertrand, F., Costa, S., Davidson, R., 2006. The western lagoon marshes of the Ria Formosa (Southern Portugal): sediment-vegetation dynamics, long-term to short-term changes and perspective. Continent. Shelf Res. 26, 363–384. https://doi.org/10.1016/j.csr.2005.12.008.

Balke, T., Stock, M., Jensen, K., Bouma, T.J., Kleyer, M., 2016. A global analysis of the seaward salt marsh extent: the importance of tidal range. Water Resour. Res. 52, 3775–3786. https://doi.org/10.1002/2015WR018318.

Barbier, E.B., Hacker, S.D., Kennedy, C., Koch, E.W., Stier, A.C., Silliman, B.R., 2011. The value of estuarine and coastal ecosystem services. Ecol. Monogr. 81, 169–193. https://doi.org/10.1890/10-1510.1.

Barbosa, C.C.A., Atkinson, P.M., Dearing, J.A., 2015. Remote sensing of ecosystem services: a systematic review. Ecol. Indicat. 52, 430–443. https://doi.org/10.1016/j.ecolind.2015.01.007.

Belluco, E., Camuffo, M., Ferrari, S., Modenese, L., Silvestri, S., Marani, A., Marani, M., 2006. Mapping salt-marsh vegetation by multispectral and hyperspectral remote sensing. Remote Sens. Environ. 105, 54–67. https://doi.org/10.1016/j.rse.2006.06.006.

Bertrand, F., Costa, S., Arnaud-Fassetta, G., Davidson, R., Beltrando, G., Goeldner-Gianella, L., Baron-Yellès, N., 2003. Dynamique des marais d'arrière-barrière associée à la passe de Barra Nova (Ria Formosa, Portugal méridional)/Evolution of backbarrier salt marshes related to the Barra Nova inlet dynamics (Ria Formosa,

south Portugal). Géomorphol. Relief, Process. Environ. 9, 151–163. https://doi.org/10.3406/morfo.2003.1176.
Best, M., Massey, A., Prior, A., 2007. Developing a saltmarsh classification tool for the European water framework directive. Mar. Pollut. Bull. 55, 205–214. https://doi.org/10.1016/j.marpolbul.2006.08.036.
Bettencourt, P., 1994. Les Environnements Sedimentaires de la Cote Sotavento (Algarve, Sud Portugal) et leur E' volution Holocene et Actuelle. University of Bordeaux.
Bortels, L., Chan, J.C.W., Merken, R., Koedam, N., 2011. Long-term monitoring of wetlands along the western-Greek bird migration route using Landsat and ASTER satellite images: amvrakikos gulf (Greece). J. Nat. Conserv. 19, 215–223. https://doi.org/10.1016/j.jnc.2011.01.004.
Brito, A.C., Quental, T., Coutinho, T.P., Branco, M.A.C., Falcão, M., Newton, A., Icely, J., Moita, T., 2012. Phytoplankton dynamics in southern Portuguese coastal lagoons during a discontinuous period of 40 years: an overview. Estuar. Coast Shelf Sci. 110, 147–156. https://doi.org/10.1016/j.ecss.2012.04.014.
Burdon, D., Potts, T., McKinley, E., Lew, S., Shilland, R., Gormley, K., Thomson, S., Forster, R., 2019. Expanding the role of participatory mapping to assess ecosystem service provision in local coastal environments. Ecosyst. Serv. 39, 101009. https://doi.org/10.1016/j.ecoser.2019.101009.
Caçador, I., Duarte, B., Marques, J.C., Sleimi, N., 2016. 6 - carbon mitigation: a salt marsh ecosystem service in times of change. In: Khan, M.A., Ozturk, M., Gul, B., Ahmed, M.Z. (Eds.), Halophytes for Food Security in Dry Lands. Academic Press, pp. 83–110. https://doi.org/10.1016/b978-0-12-801854-5.00006-6.
Campbell, A., Wang, Y., 2018. Examining the influence of tidal stage on salt marsh mapping using high-spatial-resolution satellite remote sensing and topobathymetric LiDAR. IEEE Trans. Geosci. Rem. Sens. 56, 5169–5176. https://doi.org/10.1109/TGRS.2018.2810503.
Campbell, A.D., Wang, Y., 2020. Salt marsh monitoring along the mid-Atlantic coast by Google Earth Engine enabled time series. PLoS One 15, e0229605. https://doi.org/10.1371/journal.pone.0229605.
Canisius, F., Brisco, B., Murnaghan, K., Van Der Kooij, M., Keizer, E., 2019. SAR backscatter and InSAR coherence for monitoring wetland extent, flood pulse and vegetation: a study of the amazon lowland. Rem. Sens. 11, 720. https://doi.org/10.3390/rs11060720.
Carrasco, A.R., 2019. Simple assessment of spatio-temporal evolution of salt marshes ecological services. Front. Ecol. Evol. 7, 1–7. https://doi.org/10.3389/fevo.2019.00077.
Carrasco, A.R., Kombiadou, K., Amado, M., Matias, A., 2021. Past and future marsh adaptation: lessons learned from the Ria Formosa lagoon. Sci. Total Environ. 790, 148082. https://doi.org/10.1016/j.scitotenv.2021.148082.
Chasmer, L., Cobbaert, D., Mahoney, C., Millard, K., Peters, D., Devito, K., Brisco, B., Hopkinson, C., Merchant, M., Montgomery, J., Nelson, K., Niemann, O., 2020a. Remote sensing of boreal wetlands 1: data use for policy and management. Rem. Sens. 12, 1320. https://doi.org/10.3390/rs12081320.
Chasmer, L., Mahoney, C., Millard, K., Nelson, K., Peters, D., Merchant, M., Hopkinson, C., Brisco, B., Niemann, O., Montgomery, J., Devito, K., Cobbaert, D., 2020b. Remote sensing of boreal wetlands 2: methods for evaluating boreal wetland ecosystem state and drivers of change. Rem. Sens. 12, 1321. https://doi.org/10.3390/rs12081321.
Congalton, R.G., Green, K., 2019. Assessing the accuracy of remotely sensed data. Assessing the Accuracy of Remotely Sensed Data, third ed. CRC Press, Boca Raton. https://doi.org/10.1201/9780429052729.
Contreras-Cruzado, I., Infante-Izquierdo, M.D., Márquez-García, B., Hermoso-López, V., Polo, A., Nieva, F.J.J., Cartes-Barroso, J.B., Castillo, J.M., Muñoz-Rodríguez, A., 2017. Relationships between spatio-temporal changes in the sedimentary environment and halophytes zonation in salt marshes. Geoderma 305, 173–187. https://doi.org/10.1016/j.geoderma.2017.05.037.
Correia, M., Caldwell, I.R., Koldewey, H.J., Andrade, J.P., Palma, J., 2015. Seahorse (hippocampinae) population fluctuations in the Ria Formosa lagoon, south Portugal. J. Fish. Biol. 87, 679–690. https://doi.org/10.1111/jfb.12748.
Costa, J.C., Lousã, M., Espírito-Santo, M.D., 1996. A vegetação do Parque Natural da Ria Formosa/The vegetation of "Parque Natural da Ria Formosa" (Algarve, Portugal). Stud. Bot. 15, 69–157.
Costanza, R., D'Arge, R., de Groot, R., Farber, S., Grasso, M., Hannon, B., Limburg, K., Naeem, S., O'Neill, R.V., Paruelo, J., Raskin, R.G., Sutton, P., van den Belt, M., 1997. The value of the world's ecosystem services and natural capital. Nature 387, 253–260. https://doi.org/10.1038/387253a0.
Cravo, A., Cardeira, S., Pereira, C., Rosa, M., Alcântara, P., Madureira, M., Rita, F., Luis, J., Jacob, J., 2014. Exchanges of nutrients and chlorophyll a through two inlets of Ria Formosa, South of Portugal, during coastal upwelling events. J. Sea Res. 93, 63–74. https://doi.org/10.1016/j.seares.2014.04.004.
Cunha, A.H., Santos, R.P., Gaspar, A.P., Bairros, M.F., 2005. Seagrass landscape-scale changes in response to disturbance created by the dynamics of barrier-islands: a case study from Ria Formosa (Southern Portugal). Estuar. Coast Shelf Sci. 64, 636–644. https://doi.org/10.1016/j.ecss.2005.03.018.
D'Alpaos, A., 2011. The mutual influence of biotic and abiotic components on the long-term ecomorphodynamic evolution of salt-marsh ecosystems. Geomorphology 126, 269–278. https://doi.org/10.1016/j.geomorph.2010.04.027.
D'Alpaos, A., Marani, M., 2016. Reading the signatures of biologic–geomorphic feedbacks in salt-marsh landscapes. Adv. Water Resour. 93, 265–275. https://doi.org/10.1016/j.advwatres.2015.09.004.
Da Lio, C., Teatini, P., Strozzi, T., Tosi, L., 2018. Understanding land subsidence in salt marshes of the Venice Lagoon from SAR Interferometry and ground-based investigations. Remote Sens. Environ. 205, 56–70. https://doi.org/10.1016/j.rse.2017.11.016.
Darvishzadeh, R., Wang, T., Skidmore, A., Vrieling, A., O'Connor, B., Gara, T., Ens, B., Paganini, M., 2019. Analysis of sentinel-2 and RapidEye for retrieval of leaf area index in a saltmarsh using a radiative transfer model. Rem. Sens. 11, 671. https://doi.org/10.3390/rs11060671.
DeLancey, E.R., Simms, J.F., Mahdianpari, M., Brisco, B., Mahoney, C., Kariyeva, J., 2019. Comparing deep learning and shallow learning for large-scale wetland classification in alberta, Canada. Rem. Sens. 12, 2. https://doi.org/10.3390/rs12010002.
Dubuc, B., Quiniou, J.F., Roques-Carmes, C., Tricot, C., Zucker, S.W., 1989. Evaluating the fractal dimension of profiles. Phys. Rev. A 39, 1500–1512. https://doi.org/10.1103/PhysRevA.39.1500.
Duran, J., Buades, A., Coll, B., Sbert, C., Blanchet, G., 2017. A survey of pansharpening methods with a new band-decoupled variational model. ISPRS J. Photogrammetry Remote Sens. 125, 78–105. https://doi.org/10.1016/j.isprsjprs.2016.12.013.
El Mahrad, B., Newton, A., Icely, J.D., Kacimi, I., Abalansa, S., Snoussi, M., 2020. Contribution of remote sensing technologies to a holistic coastal and marine environmental management framework: a review. Rem. Sens. 12, 2313. https://doi.org/10.3390/rs12142313.
Elsey-Quirk, T., Mariotti, G., Valentine, K., Raper, K., 2019. Retreating marsh shoreline creates hotspots of high-marsh plant diversity. Sci. Rep. 9, 5795. https://doi.org/10.1038/s41598-019-42119-8.
Eon, R.S., Goldsmith, S., Bachmann, C.M., Tyler, A.C., Lapszynski, C.S., Badura, G.P., Osgood, D.T., Brett, R., 2019. Retrieval of salt marsh above-ground biomass from high-spatial resolution hyperspectral imagery using PROSAIL. Rem. Sens. 11, 1385. https://doi.org/10.3390/rs11111385.
ESRI, 2016. ArcGIS Desktop: Release 10.5.0.6491.
European Space Agency (ESA), 2019. SNAP - ESA Sentinel Application Platform v7.0.3.
Farris, A.S., Defne, Z., Ganju, N.K., 2019. Identifying salt marsh shorelines from remotely sensed elevation data and imagery. Rem. Sens. 11, 1795. https://doi.org/10.3390/rs11151795.
Fernandez-Nunez, M., Burningham, H., Díaz-Cuevas, P., Ojeda-Zújar, J., 2019. Evaluating the response of mediterranean-atlantic saltmarshes to sea-level rise. Resources 8, 50. https://doi.org/10.3390/resources8010050.
Fisher, A., Flood, N., Danaher, T., 2016. Comparing Landsat water index methods for automated water classification in eastern Australia. Remote Sens. Environ. 175, 167–182. https://doi.org/10.1016/j.rse.2015.12.055.
Gao, Z.G., Zhang, L.Q., 2006. Multi-seasonal spectral characteristics analysis of coastal salt marsh vegetation in Shanghai, China. Estuar. Coast Shelf Sci. 69, 217–224. https://doi.org/10.1016/j.ecss.2006.04.016.
Gopi, M., Pravin Kumar, M., Joyson Joe Jeevamani, J., Raja, S., Muruganandam, R., Deepak Samuel, V., Simon, N.T., Viswanathan, C., Abhilash, K.R., Krishnan, P., Purvaja, R., Ramesh, R., 2019. Distribution and biodiversity of tropical saltmarshes: Tamil Nadu and Puducherry, Southeast coast of India. Estuar. Coast Shelf Sci. 229, 106393. https://doi.org/10.1016/j.ecss.2019.106393.
Gu, J., Luo, M., Zhang, X., Christakos, G., Agusti, S., Duarte, C.M., Wu, J., 2018. Losses of salt marsh in China: trends, threats and management. Estuar. Coast Shelf Sci. 214, 98–109. https://doi.org/10.1016/j.ecss.2018.09.015.
Guo, M., Li, J., Sheng, C., Xu, J., Wu, L., 2017. A review of wetland remote sensing. Sensors 17, 777. https://doi.org/10.3390/s17040777.
Himes-Cornell, A., Pendleton, L., Atiyah, P., 2018. Valuing ecosystem services from blue forests: a systematic review of the valuation of salt marshes, sea grass beds and mangrove forests. Ecosyst. Serv. 30, 36–48. https://doi.org/10.1016/j.ecoser.2018.01.006.
Himmelstoss, E.A., Farris, A.S., Henderson, R.E., Kratzmann, M.G., Ergul, A., Zhang, O., Zichichi, J., Thieler, E.R., 2018a. Digital Shoreline Analysis System (Version 5.0). U. S. Geological Survey software release.
Himmelstoss, E.A., Henderson, R.E., Kratzmann, M.G., Farris, A.S., 2018b. Digital Shoreline Analysis System (DSAS) Version 5.0 User Guide: U.S. Geological Survey Open-File Report 2018–1179. Woods Hole, MA. https://doi.org/10.3133/ofr20181179.
Hoggart, S., Hawkins, S.J., Bohn, K., Airoldi, L., van Belzen, J., Bichot, A., Bilton, D.T., Bouma, T.J., Colangelo, M.A., Davies, A.J., Ferrario, F., Firth, L.B., Galván, C., Hanley, M., Heurtefeux, H., Lara, J.L., Rodriguez, I.L., Maza, M., Eizaguirre, B.O., Rundle, S.D., Skov, M.W., Strain, E.M., White, A., Zhang, L., Zhu, Z., Thompson, Richard C., 2015. Ecological approaches to coastal risk mitigation. In: Zanuttigh, B., Nicholls, R., Vanderlinden, J.-P., Burcharth, H., Thompson, R.C. (Eds.), Coastal Risk Management in a Changing Climate. Butterworth-Heinemann, pp. 171–236. https://doi.org/10.1016/B978-0-12-397310-8.00004-X.
Holden, C.E., Woodcock, C.E., 2016. An analysis of Landsat 7 and Landsat 8 underflight data and the implications for time series investigations. Remote Sens. Environ. 185, 16–36. https://doi.org/10.1016/j.rse.2016.02.052.
Jabaloy-Sánchez, A., Lobo, F.J., Azor, A., Martín-Rosales, W., Pérez-Peña, J.V., Bárcenas, P., Macías, J., Fernández-Salas, L.M., Vázquez-Vílchez, M., 2014. Six thousand years of coastline evolution in the Guadalfeo deltaic system (southern Iberian Peninsula). Geomorphology 206, 374–391. https://doi.org/10.1016/j.geomorph.2013.08.037.
Jefferies, R.L., Jano, A.P., Abraham, K.F., 2006. A biotic agent promotes large-scale catastrophic change in the coastal marshes of Hudson Bay. J. Ecol. 94, 234–242. https://doi.org/10.1111/j.1365-2745.2005.01086.x.
Kelleway, J., Williams, R.J., Laegdsgaard, P., 2009. Mapping, assessment and monitoring of saltmarshes. In: Saintilan, N. (Ed.), Australian Saltmarsh Ecology. CISRO Publishing, pp. 211–230.
Kelly, M., Tuxen, K.A., Stralberg, D., 2011. Mapping changes to vegetation pattern in a restoring wetland: finding pattern metrics that are consistent across spatial scale and time. Ecol. Indicat. 11, 263–273. https://doi.org/10.1016/j.ecolind.2010.05.003.

Klemas, V., 2011. Remote sensing of wetlands: case studies comparing practical techniques. J. Coast Res. 27, 418. https://doi.org/10.2112/jcoastres-d-10-00174.1.
Klemas, V., 2013a. Remote sensing of coastal wetland biomass: an overview. J. Coast Res. 290, 1016–1028. https://doi.org/10.2112/JCOASTRES-D-12-00237.1.
Klemas, V., 2013b. Using remote sensing to select and monitor wetland restoration sites: an overview. J. Coast Res. 289, 958–970. https://doi.org/10.2112/JCOASTRES-D-12-00170.1.
Knight, D., LeDrew, E., Holden, H., 1997. Mapping submerged corals in Fiji from remote sensing and in situ measurements: applications for integrated coastal management. Ocean Coast Manag. 34, 153–170. https://doi.org/10.1016/S0964-5691(97)00001-X.
Kombiadou, K., Matias, A., Carrasco, R., Ferreira, Ó., Costas, S., Vieira, G., 2018. Towards assessing the resilience of complex coastal systems: examples from Ria Formosa (south Portugal). J. Coast Res. 646–650. https://doi.org/10.2112/SI85-130.1.
Kombiadou, K., Matias, A., Ferreira, Ó., Carrasco, A.R., Costas, S., Plomaritis, T., 2019. Impacts of human interventions on the evolution of the Ria Formosa barrier island system (S. Portugal). Geomorphology 343, 129–144. https://doi.org/10.1016/j.geomorph.2019.07.006.
Laengner, M.L., Siteur, K., van der Wal, D., 2019. Trends in the seaward extent of saltmarshes across europe from long-term satellite data. Rem. Sens. 11, 1653. https://doi.org/10.3390/rs11141653.
Leonardi, N., Defne, Z., Ganju, N.K., Fagherazzi, S., 2016. Salt marsh erosion rates and boundary features in a shallow Bay. J. Geophys. Res. Earth Surf. 121, 1861–1875. https://doi.org/10.1002/2016JF003975.
Li, H., Wan, W., Fang, Y., Zhu, S., Chen, X., Liu, B., Hong, Y., 2019. A Google Earth Engine-enabled software for efficiently generating high-quality user-ready Landsat mosaic images. Environ. Model. Software 112, 16–22. https://doi.org/10.1016/j.envsoft.2018.11.004.
Lillebø, A.I., Sousa, A.I., Flindt, M.R., Pereira, M.E., Duarte, A.C., Pardal, M.A., Caçador, I., 2010. Nutrient cycling in salt marshes: an ecosystem service to reduce eutrophication. In: Webber, C.D. (Ed.), Eutrophication: Ecological Effects, Sources, Prevention and Reversal. Nova Science Publishers, Inc., New York, pp. 135–160.
Lopes, C.L., Mendes, R., Caçador, I., Dias, J.M., 2019. Evaluation of long-term estuarine vegetation changes through Landsat imagery. Sci. Total Environ. 653, 512–522. https://doi.org/10.1016/j.scitotenv.2018.10.381.
Lopes, C.L., Mendes, R., Caçador, I., Dias, J.M., 2020. Assessing salt marsh extent and condition changes with 35 years of Landsat imagery: tagus Estuary case study. Remote Sens. Environ. 247, 111939. https://doi.org/10.1016/j.rse.2020.111939.
Louis, J., 2017. S2 MPC - L2A Product Definition Document (Ref. S2-PDGS-MPC-L2A-PDD-V14.2). ESA.
Maes, J., Teller, A., Nessi, S., Bulgheroni, C., Konti, A., Sinkko, T., Tonini, D., Pant, R., Erhard, M., Condé, S., Vallecillo, S., Barredo, J.I., Paracchini, M.L., Abdul Malak, D., Trombetti, M., Vigiak, O., Zulian, G., Addamo, A.M., Grizzetti, B., Somma, F., Hagyo, A., Vogt, P., Polce, C., Jones, A., Marin, A.I., Ivits, E., Mauri, A., Rega, C., Czúcz, B., Ceccherini, G., Pisoni, E., Ceglar, A., De Palma, P., Cerrani, I., Meroni, M., Caudullo, G., Lugato, E., Vogt, J.V., Spinoni, J., Cammalleri, C., Bastrup-Birk, A., San Miguel, J., San Román, S., Kristensen, P., Christiansen, T., Zal, N., de Roo, A., Cardoso, A.C., Pistocchi, A., Del Barrio Alvarellos, I., Tsiamis, K., Gervasini, E., Deriu, I., La Notte, A., Abad Viñas, R., Vizzarri, M., Camia, A., Robert, N., Kakoulaki, G., Garcia Bendito, E., Panagos, P., Ballabio, C., Scarpa, S., Montanarella, L., Orgiazzi, A., Fernandez Ugalde, O., Santos-Martín, F., 2020. Annex Mapping and Assessment of Ecosystems and Their Services: an EU Ecosystem Assessment, JRC Science for Policy Reports. European Commission. European Union, Ispra. https://doi.org/10.2760/757183.
Mahdianpari, M., Salehi, B., Mohammadimanesh, F., Homayouni, S., Gill, E., 2019. The first wetland inventory map of newfoundland at a spatial resolution of 10 m using sentinel-1 and sentinel-2 data on the Google Earth Engine cloud computing platform. Rem. Sens. 11 https://doi.org/10.3390/rs11010043.
Mao, D., Wang, Z., Du, B., Li, L., Tian, Y., Jia, M., Zeng, Y., Song, K., Jiang, M., Wang, Y., 2020. National wetland mapping in China: a new product resulting from object-based and hierarchical classification of Landsat 8 OLI images. ISPRS J. Photogrammetry Remote Sens. 164, 11–25. https://doi.org/10.1016/j.isprsjprs.2020.03.020.
Marani, M., Silvestri, S., Belluco, E., Ursino, N., Comerlati, A., Tosatto, O., Putti, M., 2006a. Spatial organization and ecohydrological interactions in oxygen-limited vegetation ecosystems. Water Resour. Res. 42, 1–12. https://doi.org/10.1029/2005WR004582.
Marani, M., Belluco, E., Ferrari, S., Silvestri, S., D'Alpaos, A., Lanzoni, S., Feola, A., Rinaldo, A., 2006b. Analysis, synthesis and modelling of high-resolution observations of salt-marsh eco-geomorphological patterns in the Venice lagoon. Estuar. Coast Shelf Sci. 69, 414–426. https://doi.org/10.1016/j.ecss.2006.05.021.
Materu, S.F., Urban, B., Heise, S., 2018. A critical review of policies and legislation protecting Tanzanian wetlands. Ecosys. Health Sustain. 4, 310–320. https://doi.org/10.1080/20964129.2018.1549510.
Mateus, M., Almeida, D., Simonson, W., Felgueiras, M., Banza, P., Batty, L., 2016. Conflictive uses of coastal areas: a case study in a southern European coastal lagoon (Ria de Alvor, Portugal). Ocean Coast Manag. 132, 90–100. https://doi.org/10.1016/j.ocecoaman.2016.08.016.
Mcowen, C., Weatherdon, L., Bochove, J.-W., Sullivan, E., Blyth, S., Zockler, C., Stanwell-Smith, D., Kingston, N., Martin, C., Spalding, M., Fletcher, S., 2017. A global map of saltmarshes. Biodivers. Data J. 5, e11764 https://doi.org/10.3897/BDJ.5.e11764.
Meng, X., Shen, H., Li, H., Zhang, L., Fu, R., 2019. Review of the pansharpening methods for remote sensing images based on the idea of meta-analysis: practical discussion and challenges. Inf. Fusion 46, 102–113. https://doi.org/10.1016/j.inffus.2018.05.006.
Mitsch, W.J., Gosselink, J.G., 2015. Tidal marshes. In: Wetlands. John Wiley & Sons Inc, Hoboken, NJ, pp. 259–310.
Moffett, K., Nardin, W., Silvestri, S., Wang, C., Temmerman, S., 2015. Multiple stable states and catastrophic shifts in coastal wetlands: progress, challenges, and opportunities in validating theory using remote sensing and other methods. Rem. Sens. 7, 10184–10226. https://doi.org/10.3390/rs70810184.
Moreira Da Silva, M., Aníbal, J., Duarte, D., Chícharo, L., 2015. Sarcocornia fruticosa and spartina maritima as heavy metals remediators in Southwestern European Salt Marsh (Ria Formosa, Portugal). J. Environ. Prot. Ecol. 16, 1468–1477.
Morton, R.A., Miller, T.L., Moore, L.J., 2004. National Assessment of Shoreline Change: Part 1: Historical Shoreline Changes and Associated Coastal Land Loss along the US Gulf of Mexico: U.S. Gulf of Mexico: U.S. Geological Survey Open-File Report 2004-1043. St. Petersburg, FL.
Muller-Karger, F.E., Hestir, E., Ade, C., Turpie, K., Roberts, D.A., Siegel, D., Miller, R.J., Humm, D., Izenberg, N., Keller, M., Morgan, F., Frouin, R., Dekker, A.G., Gardner, R., Goodman, J., Schaeffer, B., Franz, B.A., Pahlevan, N., Mannino, A.G., Concha, J.A., Ackleson, S.G., Cavanaugh, K.C., Romanou, A., Tzortziou, M., Boss, E.S., Pavlick, R., Freeman, A., Rousseaux, C.S., Dunne, J., Long, M.C., Klein, E., McKinley, G.A., Goes, J., Letelier, R., Kavanaugh, M., Roffer, M., Bracher, A., Arrigo, K.R., Dierssen, H., Zhang, X., Davis, F.W., Best, B., Guralnick, R., Moisan, J., Sosik, H.M., Kudela, R., Mouw, C.B., Barnard, A.H., Palacios, S., Roesler, C., Drakou, E.G., Appeltans, W., Jetz, W., 2018. Satellite sensor requirements for monitoring essential biodiversity variables of coastal ecosystems. Ecol. Appl. 28, 749–760. https://doi.org/10.1002/eap.1682.
Müllerová, J., Brůna, J., Bartaloš, T., Dvořák, P., Vítková, M., Pyšek, P., 2017. Timing is important: unmanned aircraft vs. Satellite imagery in plant invasion monitoring. Front. Plant Sci. 8, 1–13. https://doi.org/10.3389/fpls.2017.00887.
Mumby, P.J., Green, E.P., Edwards, A.J., Clark, C.D., 1999. The cost-effectiveness of remote sensing for tropical coastal resources assessment and management. J. Environ. Manag. 55, 157–166. https://doi.org/10.1006/jema.1998.0255.
Nayak, S., 2004. Role of remote sensing in integrated coastal zone management. Int. Arch. Photogramm. Remote Sens. Spat. Inf. Sci. - ISPRS Arch. 35, 1232–1243.
Newton, A., Brito, A.C., Icely, J.D., Derolez, V., Clara, I., Angus, S., Schernewski, G., Inácio, M., Lillebø, A.I., Sousa, A.I., Béjaoui, B., Solidoro, C., Tosic, M., Cañedo-Argüelles, M., Yamamuro, M., Reizopoulou, S., Tseng, H.-C., Canu, D., Roselli, L., Maanan, M., Cristina, S., Ruiz-Fernández, A.C., Lima, R.F. d. de, Kjerfve, B., Rubio-Cisneros, N., Pérez-Ruzafa, A., Marcos, C., Pastres, R., Pranovi, F., Snoussi, M., Turpie, J., Tuchkovenko, Y., Dyack, B., Brookes, J., Povilanskas, R., Khokhlov, V., 2018. Assessing, quantifying and valuing the ecosystem services of coastal lagoons. J. Nat. Conserv. 44, 50–65. https://doi.org/10.1016/j.jnc.2018.02.009.
Niu, Z., Zhang, H., Wang, X., Yao, W., Zhou, D., Zhao, K., Zhao, H., Li, N., Huang, H., Li, C., Yang, J., Liu, C., Liu, S., Wang, L., Li, Z., Yang, Z., Qiao, F., Zheng, Y., Chen, Y., Sheng, Y., Gao, X., Zhu, W., Wang, W., Wang, H., Weng, Y., Zhuang, D., Liu, J., Luo, Z., Cheng, X., Guo, Z., Gong, P., 2012. Mapping wetland changes in China between 1978 and 2008. Chin. Sci. Bull. 57, 2813–2823. https://doi.org/10.1007/s11434-012-5093-3.
Ouellette, W., Getinet, W., 2016. Remote sensing for marine spatial planning and integrated coastal areas management: achievements, challenges, opportunities and future prospects. Remote Sens. Appl. Soc. Environ. 4, 138–157. https://doi.org/10.1016/j.rsase.2016.07.003.
Pacheco, A., Vila-Concejo, A., Ferreira, Ó., Dias, J.A., 2008. Assessment of tidal inlet evolution and stability using sediment budget computations and hydraulic parameter analysis. Mar. Geol. 247, 104–127. https://doi.org/10.1016/j.margeo.2007.07.003.
Perennou, C., Guelmami, A., Paganini, M., Philipson, P., Poulin, B., Strauch, A., Tottrup, C., Truckenbrodt, J., Geijzendorffer, I.R., 2018. Mapping mediterranean wetlands with remote sensing: a good-looking map is not always a good map. In: Advances in Ecological Research. Elsevier Ltd, pp. 243–277. https://doi.org/10.1016/bs.aecr.2017.12.002.
Pham, T.D., Xia, J., Ha, N.T., Bui, D.T., Le, N.N., Tekeuchi, W., 2019. A review of remote sensing approaches for monitoring blue carbon ecosystems: mangroves, seagrassesand salt marshes during 2010–2018. Sensors 19, 1933. https://doi.org/10.3390/s19081933.
Qu, J.J., Gao, W., Kafatos, M., Murphy, R.E., Salomonson, V.V., 2006. Earth science satellite remote sensing. In: Data, Computational Processing, and Tools, vol. 2. Springer Berlin Heidelberg, Berlin Heidelberg. https://doi.org/10.1007/978-3-540-37294-3.
Read, J.M., Chambers, C., Torrado, M., 2020. Remote sensing. In: International Encyclopedia of Human Geography. Elsevier, pp. 411–422. https://doi.org/10.1016/B978-0-08-102295-5.10589-X.
Rebelo, A.J., Scheunders, P., Esler, K.J., Meire, P., 2017. Detecting, mapping and classifying wetland fragments at a landscape scale. Remote Sens. Appl. Soc. Environ. 8, 212–223. https://doi.org/10.1016/j.rsase.2017.09.005.
Reboreda, R., Caçador, I., 2007. Halophyte vegetation influences in salt marsh retention capacity for heavy metals. Environ. Pollut. 146, 147–154. https://doi.org/10.1016/j.envpol.2006.05.035.
Reed, D., van Wesenbeeck, B., Herman, P.M.J., Meselhe, E., 2018. Tidal flat-wetland systems as flood defenses: understanding biogeomorphic controls. Estuar. Coast Shelf Sci. 213, 269–282. https://doi.org/10.1016/j.ecss.2018.08.017.
Reschke, J., Hüttich, C., 2014. Continuous field mapping of Mediterranean wetlands using sub-pixel spectral signatures and multi-temporal Landsat data. Int. J. Appl. Earth Obs. Geoinf. 28, 220–229. https://doi.org/10.1016/j.jag.2013.12.014.
Rogers, K., Boon, P.I., Branigan, S., Duke, N.C., Field, C.D., Fitzsimons, J.A., Kirkman, H., Mackenzie, J.R., Saintilan, N., 2016. The state of legislation and policy protecting Australia's mangrove and salt marsh and their ecosystem services. Mar. Pol. 72, 139–155. https://doi.org/10.1016/j.marpol.2016.06.025.

Roy, D.P., Wulder, M.A., Loveland, T.R., Woodcock, C.E, Allen, R.G., Anderson, M.C., Helder, D., Irons, J.R., Johnson, D.M., Kennedy, R., Scambos, T.A., Schaaf, C.B., Schott, J.R., Sheng, Y., Vermote, E.F., Belward, A.S., Bindschadler, R., Cohen, W.B., Gao, F., Hipple, J.D., Hostert, P., Huntington, J., Justice, C.O., Kilic, A., Kovalskyy, V., Lee, Z.P., Lymburner, L., Masek, J.G., McCorkel, J., Shuai, Y., Trezza, R., Vogelmann, J., Wynne, R.H., Zhu, Z., 2014. Landsat-8: science and product vision for terrestrial global change research. Remote Sens. Environ. 145, 154–172. https://doi.org/10.1016/j.rse.2014.02.001.

Ruggiero, P., Kratzmann, M.G., Himmelstoss, E.A., Reid, D., Allan, J., Kaminsky, G., 2013. National Assessment of Shoreline Change-Historical Shoreline Change along the Pacific Northwest Coast: U.S. Geological Survey Open-File Report 2012-1007. U. S. Environmental Protection Agency, Virginia. https://doi.org/10.3133/ofr20121007.

Ryfield, F., Cabana, D., Brannigan, J., Crowe, T., 2019. Conceptualizing 'sense of place' in cultural ecosystem services: a framework for interdisciplinary research. Ecosyst. Serv. 36, 100907. https://doi.org/10.1016/j.ecoser.2019.100907.

Siegenthaler, A., Cánovas, F., González-Wangüemert, M., 2015. Spatial distribution patterns and movements of Holothuria arguinensis in the Ria Formosa (Portugal). J. Sea Res. 102, 33–40. https://doi.org/10.1016/j.seares.2015.04.003.

Silvestri, S., D'Alpaos, A., Nordio, G., Carniello, L., 2018. Anthropogenic modifications can significantly influence the local mean sea level and affect the survival of salt marshes in shallow tidal systems. J. Geophys. Res. Earth Surf. 123, 996–1012. https://doi.org/10.1029/2017JF004503.

Silvestri, S., Marani, M., Marani, A., 2003. Hyperspectral remote sensing of salt marsh vegetation, morphology and soil topography. Phys. Chem. Earth, Parts A/B/C 28, 15–25. https://doi.org/10.1016/S1474-7065(03)00004-4.

Sivakumar, R., Ghosh, S., 2016. Wetland spatial dynamics and mitigation study: an integrated remote sensing and GIS approach. Nat. Hazards 80, 975–995. https://doi.org/10.1007/s11069-015-2007-0.

Sousa, A.I., Lillebø, A.I., Pardal, M.A., Caçador, I., 2010. Productivity and nutrient cycling in salt marshes: contribution to ecosystem health. Estuar. Coast Shelf Sci. 87, 640–646. https://doi.org/10.1016/j.ecss.2010.03.007.

Sousa, C.A.M., Boski, T., Pereira, L., 2019. Holocene evolution of a barrier island system, Ria Formosa, South Portugal. Holocene 29, 64–76. https://doi.org/10.1177/0959683618804639.

Sousa, C.A.M., Cunha, M.E., Ribeiro, L., 2020. Tracking 130 years of coastal wetland reclamation in Ria Formosa, Portugal: opportunities for conservation and aquaculture. Land Use Pol. 94, 104544. https://doi.org/10.1016/j.landusepol.2020.104544.

Sun, C., Fagherazzi, S., Liu, Y., 2018. Classification mapping of salt marsh vegetation by flexible monthly NDVI time-series using Landsat imagery. Estuar. Coast Shelf Sci. 213, 61–80. https://doi.org/10.1016/j.ecss.2018.08.007.

Sun, X., Li, Y., Zhu, X., Cao, K., Feng, L., 2017. Integrative assessment and management implications on ecosystem services loss of coastal wetlands due to reclamation. J. Clean. Prod. 163, S101–S112. https://doi.org/10.1016/j.jclepro.2015.10.048.

Taramelli, A., Valentini, E., Cornacchia, L., Monbaliu, J., Sabbe, K., 2018. Indications of dynamic effects on scaling relationships between channel sinuosity and vegetation patch size across a salt marsh platform. J. Geophys. Res. Earth Surf. 123, 2714–2731. https://doi.org/10.1029/2017JF004540.

Tian, B., Zhou, Y.-X., Thom, R.M., Diefenderfer, H.L., Yuan, Q., 2015. Detecting wetland changes in Shanghai, China using FORMOSAT and Landsat TM imagery. J. Hydrol. 529, 1–10. https://doi.org/10.1016/j.jhydrol.2015.07.007.

Turpie, K.R., Klemas, V.V., Byrd, K., Kelly, M., Jo, Y.-H., 2015. Prospective HyspIRI global observations of tidal wetlands. Remote Sens. Environ. 167, 206–217. https://doi.org/10.1016/j.rse.2015.05.008.

U.S. Geological Survey, 2019a. Landsat 8 Surface Reflectance Code (LASRC) Product Guide. (No. LSDS-1368 Version 2.0). EROS, Sioux Falls, SD.

U.S. Geological Survey, 2019b. Landsat 4-7 Surface Reflectance (LEDAPS) Product Guide. EROS, Sioux Falls, SD.

U.S. Geological Survey, 2019c. Landsat Collection 1 Level 1 Product Definition (LSDS-1656 Version 2.0). EROS, Sioux Falls, SD.

U.S. Geological Survey, 2018. Landsat Multispectral Scanner (MSS) Level 1 (L1) Data Format Control Book (DFCB) (LSDS-286 Version 11.0), LSDS-286 Version 11.0. EROS, Sioux Falls, SD.

Valiela, I., Kinney, E., Culbertson, J., Peacock, E., Smith, S., 2009. Global losses of mangroves and salt marshes. In: Duarte, C.M. (Ed.), Global Loss of Coastal Habitats Rates, Causes and Consequences. Fundación BBVA, p. 142.

Valiela, I., Lloret, J., Bowyer, T., Miner, S., Remsen, D., Elmstrom, E., Cogswell, C., Robert Thieler, E., 2018. Transient coastal landscapes: rising sea level threatens salt marshes. Sci. Total Environ. 640–641, 1148–1156. https://doi.org/10.1016/j.scitotenv.2018.05.235.

Vernberg, F.J., 1993. Salt-marsh processes: a review. Environ. Toxicol. Chem. 12, 2167–2195. https://doi.org/10.1002/etc.5620121203.

Vivone, G., Alparone, L., Chanussot, J., Dalla Mura, M., Garzelli, A., Licciardi, G.A., Restaino, R., Wald, L., 2015. A critical comparison among pansharpening algorithms. IEEE Trans. Geosci. Rem. Sens. 53, 2565–2586. https://doi.org/10.1109/TGRS.2014.2361734.

Vogelmann, J.E., Gallant, A.L., Shi, H., Zhu, Z., 2016. Perspectives on monitoring gradual change across the continuity of Landsat sensors using time-series data. Remote Sens. Environ. 185, 258–270. https://doi.org/10.1016/j.rse.2016.02.060.

Waldner, F., Duveiller, G., Defourny, P., 2018. Local adjustments of image spatial resolution to optimize large-area mapping in the era of big data. Int. J. Appl. Earth Obs. Geoinf. 73, 374–385. https://doi.org/10.1016/j.jag.2018.07.009.

Wu, Q., 2018. GIS and remote sensing applications in wetland mapping and monitoring. In: Comprehensive Geographic Information Systems. Elsevier, pp. 140–157. https://doi.org/10.1016/B978-0-12-409548-9.10460-9.

Wu, W., 2019. Accounting for spatial patterns in deriving sea-level rise thresholds for salt marsh stability: more than just total areas? Ecol. Indicat. 103, 260–271. https://doi.org/10.1016/j.ecolind.2019.04.008.

Young, N.E., Anderson, R.S., Chignell, S.M., Vorster, A.G., Lawrence, R., Evangelista, P. H., 2017. A survival guide to Landsat preprocessing. Ecology 98, 920–932. https://doi.org/10.1002/ecy.1730.

Zhang, H., Roy, D., 2016. Computationally inexpensive Landsat 8 operational land imager (OLI) pansharpening. Rem. Sens. 8, 180. https://doi.org/10.3390/rs8030180.

Zhu, Z., Wulder, M.A., Roy, D.P., Woodcock, C.E., Hansen, M.C., Radeloff, V.C., Healey, S.P., Schaaf, C., Hostert, P., Strobl, P., Pekel, J.-F., Lymburner, L., Pahlevan, N., Scambos, T.A., 2019. Benefits of the free and open Landsat data policy. Remote Sens. Environ. 224, 382–385. https://doi.org/10.1016/j.rse.2019.02.016.